Self Calibration of Tomographic Weak Lensing for the Physics of Baryons to Constrain Dark Energy

Andrew R. Zentner,[1,2,3] Douglas H. Rudd,[2] and Wayne Hu[2,3]

[1] *Department of Physics and Astronomy, University of Pittsburgh, Pittsburgh, PA 15260* *
[2] *Kavli Institute for Cosmological Physics and Department of Astronomy and Astrophysics, The University of Chicago, Chicago, IL 60637*
[3] *The Enrico Fermi Institute, The University of Chicago, Chicago, IL 60637*

(Dated: February 2, 2008)

Recent numerical studies indicate that uncertainties in the treatment of baryonic physics can affect predictions for weak lensing shear power spectra at a level that is significant for several forthcoming surveys such as the Dark Energy Survey (DES), the SuperNova/Acceleration Probe (SNAP), and the Large Synoptic Survey Telescope (LSST). Correspondingly, we show that baryonic effects can significantly bias dark energy parameter measurements. Elimination of such potential biases by neglecting information in multipoles beyond several hundred leads to weaker parameter constraints by a factor of $\sim 2-3$ compared with using information out to multipoles of several thousand. Fortunately, the same numerical studies that explore the influence of baryons indicate that they primarily affect power spectra by altering halo structure through the relation between halo mass and mean effective halo concentration. We explore the ability of future weak lensing surveys to constrain both the internal structures of halos and the properties of the dark energy simultaneously as a first step toward self calibrating for the physics of baryons. In this approach, parameter biases are greatly reduced and no parameter constraint is degraded by more than $\sim 40\%$ in the case of LSST or 30% in the cases of SNAP or DES. Modest prior knowledge of the halo concentration relation and its redshift evolution greatly improves even these forecasts. In addition, we find that these surveys can constrain effective halo concentrations themselves usefully with shear power spectra alone. In the most restrictive case of a power-law relation for halo concentration as a function of mass and redshift, the concentrations of halos of mass $m \sim 10^{14}\ h^{-1}\mathrm{M}_\odot$ at $z \sim 0.2$ can be constrained to better than 10%. Our results suggest that inferring dark energy parameters through shear spectra can be made robust to baryonic physics and that this procedure may even provide useful constraints on galaxy formation models.

PACS numbers: 98.80.-k,98.62.Py,98.35.Gi

I. INTRODUCTION

An ever-expanding set of observational data indicate that roughly $\sim 75\%$ of the energy in the universe is in the form of *dark energy* whose negative pressure drives an accelerated cosmological expansion (e.g., [1, 2, 3, 4, 5, 6, 7, 8, 9]). Determining the nature of the dark energy is one of the most profound problems facing physicists and astronomers. Numerous contemporary and forthcoming experiments aim to shed light on the dark energy problem using a variety of techniques. One of the most promising probes of dark energy is weak gravitational lensing. Forthcoming weak lensing surveys expect to measure the statistics of the matter density fluctuation field with exquisite precision. Dark energy affects both the rate of structure growth and the relative angular diameter distances between different redshifts and so these precise determinations of the matter fluctuation spectrum bring the promise of stringent constraints on dark energy parameters [10, 11, 12, 13, 14, 15, 16, 17, 18, 19, 20, 21].

Of course, exploiting precise measurements of fluctuations in the density field to constrain dark energy requires precise predictions for these inhomogeneities. Maximizing the constraining power of future surveys in this regard demands that predictions for the linear and nonlinear matter power spectra be accurate at the percent level [22, 23]. This remains a challenge for numerical simulations even in the absence of baryonic physics [24], but this challenge should yield to unrelenting increases in computational power. Perhaps more important is the treatment of the baryonic component of the universe. Early analytic studies indicated that baryonic processes may have a significant influence on shear power spectra [25, 26]. More recently, Jing et al. [27] and Rudd et al. [28] showed that numerical simulations that include baryonic processes predict matter power spectra that differ from those that result from dissipationless N-body calculations at a level that exceeds the precision of various forthcoming experiments. The evolution of the baryonic component of the universe cannot be modeled directly with current computational limitations and this circumstance is unlikely to yield to increases in computational power in the foreseeable future. As a consequence, all calculations rely on effective models that attempt to approximate the net, large-scale influences of numerous processes that occur on scales far below the numerical resolution that may be attained with any simulation. The implication of Refs. [27, 28] is that the ability of weak

*Electronic address: zentner@pitt.edu

lensing surveys to constrain dark energy parameters may be severely limited by this inability to account for baryonic processes reliably.

The goal of this study is to investigate this implication. In particular, we aim to determine if measurements of shear power spectra (including tomography with photometric redshifts) contain sufficient information to constrain both the influence of baryons and the properties of the dark energy. Rudd et al. [28] found that the influence of baryons is due almost entirely to modifications in the matter distribution within dark matter halos. We model the influence of baryons in this way, so our calculation is tantamount to determining the ability of future surveys to constrain a physically-motivated model for the density profiles of dark matter halos and dark energy parameters simultaneously. Naturally, gravitational lensing is sensitive to all matter along the lines of sight to sources. In the following we refer to the distribution of mass within halos for simplicity, but we do not intend to restrict our consideration to the dark matter. We use this terminology as a shorthand to refer to the total mass distribution of the composite dark matter and baryonic systems within halo virial radii.

Our results suggest that forthcoming surveys will have sufficient information to calibrate for the influence of baryons on the matter power spectrum using weak lensing shear power spectra alone, with minimal degradation in the constraints on dark energy parameters. In fact, we study models that are quite general so our results suggest that such surveys can also calibrate additional systematics that may afflict a similar range of scales. Of course, one need not regard halo structure strictly as a nuisance. An interesting concomitant outcome of this calibration program is that weak lensing surveys will provide constraints on halo structure that complement constraints obtained via alternative means (e.g., Ref. [29, 30, 31, 32, 33, 34, 35, 36]). This byproduct of dark energy studies extends the scientific reach of future surveys as it may prove useful to inform models of the formation of galaxies and galaxy clusters.

Alongside this success, we emphasize that our results must be considered with some circumspection. Though it appears to be the dominant effect, we do not expect that the influence of baryons is strictly limited to the internal structures of halos. In our study we also neglect all systematics other than baryonic physics, such as intrinsic alignments [37, 38, 39, 40]. We consider this exercise to be a proof of concept indicating that self calibration is achievable at minimal cost and that weak lensing tomography may constrain halo profiles at interesting levels.

There are several papers in the literature that are closely related to our work. We have already mentioned that both White [25] and Zhan and Knox [26] studied the effects of baryons on convergence spectra using analytic models and indicated that they will likely be non-negligible, at least over some range of scales. Though prescient, both of these studies are based on phenomenological models that do not treat all of the effects of baryons self consistently, while the study of Zhan and Knox [26] focuses on the influence of hot baryons and neglect baryonic cooling. The result of these studies is that baryonic processes influence lensing observables on scales near $\ell \sim 10^3$ at a level below that reported in Refs. [27, 28]. Furthermore, it is not entirely surprising that the information within forthcoming lensing surveys suffices to calibrate additional physics, such as the influence of baryonic processes. Huterer et al. [23] studied self calibration of multiplicative and additive observational systematics and found that these could be calibrated successfully at a relatively low cost. Self calibration of systematics, including intrinsic alignment effects is also discussed briefly in the appendices of the report of the Dark Energy Task Force (DETF, Ref. [41]) and such self calibration is included in their analyses.

We describe our methods in the following section. We begin with a review of weak lensing tomography. Next, we summarize the salient features of the halo model for nonlinear clustering. We then review the Fisher matrix formalism for assessing the constraining power of forthcoming experiments and mention some of the specifics of our implementation, including our fiducial model and priors. We close the second section with a variety of models that we use to incorporate parameterized baryonic physics into our calculations.

In Section III, we present the results of our study. We open with a review of forecasts for dark energy constraints in the absence of any unknown baryonic physics. The results of this exercise represent constraints in the limit of perfect knowledge of halo profiles and correspond directly to other forecasts in the literature. This limit serves as a useful reference for interpreting subsequent parameter constraints. Following this, we give forecasts for dark energy parameter constraints after including and marginalizing over the contribution of unknown baryonic physics. We continue with constraints on halo profiles themselves after marginalizing over dark energy. Our final results show dark energy constraints behave as a function of external, independent constraints on halo profiles that can be included in the analysis. We discuss our results, including caveats and avenues for future study, and draw conclusions in Section IV.

II. METHODS

A. Weak Lensing Observables

In this study, we consider utilizing information in weak lensing observables only. We model our approach after that of Ma et al. [42]. In particular, we consider convergence power spectra from $N_{\rm TOM}$ tomographic redshift bins defined by the photometric redshifts of source galaxies. The $N_{\rm TOM}(N_{\rm TOM}+1)/2$ observables given by the number density-weighted convergence spectra and cross spectra for the tomographic bins as a function of multi-

pole ℓ, are

$$P_\kappa^{\rm ij}(\ell) = \int {\rm d}z \frac{W_{\rm i}(z) W_{\rm j}(z)}{H(z) D_{\rm A}^2(z)} P(k = \ell/D_{\rm A}, z). \quad (1)$$

In Eq. (1), $H(z)$ is the Hubble expansion rate, $D_{\rm A}$ is the angular diameter distance, and $P(k, z)$ is the three-dimensional total matter power spectrum at wavenumber k and redshift z. The lensing weight functions $W_{\rm i}(z)$ specify the tomographic bins. Defining the true redshift distribution of source galaxies in the ith photometric redshift bin as ${\rm d}n_{\rm i}/{\rm d}z$, the lensing weight functions are given by

$$W_{\rm i}(z) = \frac{3}{2}\Omega_{\rm M} H_0^2 (1+z) D_{\rm A}(z) \int {\rm d}z' \frac{D_{\rm A}(z, z')}{D_{\rm A}(z')} \frac{{\rm d}n_{\rm i}}{{\rm d}z'}. \quad (2)$$

The present Hubble rate is H_0 and $D_{\rm A}(z, z')$ denotes the angular diameter distance between redshifts z and z'. Note that the source distribution is not normalized to integrate to unity and hence $P_\kappa^{\rm ij}$ represents the power spectra weighted by the product of angular number densities in the ith and jth photometric redshift bins.

It is natural to express the photometric redshift bins in terms of the total true redshift distribution of source galaxies ${\rm d}n/{\rm d}z$, and the probability of yielding a photometric redshift $z_{\rm p}$ given a true redshift z, which we denote $P(z_{\rm p}|z)$. In this case, the true redshift distribution of sources in the ith photometric redshift bin can be obtained by integrating between the photometric redshift limits of the bin

$$\frac{{\rm d}n_{\rm i}(z)}{{\rm d}z} = \int_{z_{\rm i}^{\rm low}}^{z_{\rm i}^{\rm high}} {\rm d}z_{\rm p} \frac{{\rm d}n(z)}{{\rm d}z} P(z_{\rm p}|z). \quad (3)$$

For the purpose of this study, we take the true redshift distribution to be

$$\frac{{\rm d}n(z)}{{\rm d}z} = \bar{n} \frac{4z^2}{\sqrt{2\pi} z_0^3} \exp[-(z/z_0)^2] \quad (4)$$

with $z_0 \simeq 0.92$, which fixes the median survey redshift to $z_{\rm med} = 1$. The parameter $\bar{n}$ represents the total density of source galaxies per unit of solid angle. For simplicity and concreteness, we model the photometric redshift distribution as in `Model I` of Ref. [42]. To be specific, we take $P(z_{\rm p}|z)$ to be a Gaussian centered at $z_{\rm p} = z$ with dispersion $\sigma_z = 0.05(1+z)$. We define tomographic bins to be evenly spaced in redshift from $z = 0$ to $z = 3$, putting whatever fraction (of order $\sim 10^{-4}$) of galaxies that lie beyond $z = 3$ into the highest redshift tomographic bin. We number our tomographic bins sequentially so that 1 designates the lowest redshift bin and $N_{\rm TOM}$ labels the highest redshift bin. Unless we state otherwise, we report results with $N_{\rm TOM} = 5$ as we find little relative improvement in parameter constraints with finer tomographic binning, in agreement with previous work [42].

B. A Halo Model Primer

To evaluate the relations in Section II A, it is necessary to compute the nonlinear matter power spectrum. Though other methods exist and have proven quite successful [43, 44], we use the phenomenological halo model to accomplish this. Elements of the halo model have been developed in a number of studies [45, 46, 47, 48, 49]. A comprehensive review can be found in Ref. [50]. We implement the halo model as in Rudd et al. [28] and review the salient features below.

The halo model is predicated on the assumption that all matter resides within dark matter halos. The matter power spectrum is given by a sum of two terms,

$$P(k) = P_{\rm 1H}(k) + P_{\rm 2H}(k). \quad (5)$$

The first term is from matter elements that reside within a common dark matter halo, while the second term is due to elements that reside in distinct dark matter halos. The utility of this decomposition in the present context is apparent. Baryonic processes have a significant influence on the structures of individual dark matter halos, but have little effect on the large-scale clustering of halos themselves and these ingredients are treated independently in the halo model.

The one-halo contribution is

$$P_{\rm 1H}(k) = \frac{1}{\rho_{\rm M}^2} \int {\rm d}m \; m^2 \frac{{\rm d}n}{{\rm d}m} \lambda^2(k, m), \quad (6)$$

where $\rho_{\rm M}$ is the mean matter density of the universe, m is halo mass, ${\rm d}n/{\rm d}m$ is the mass function of dark matter halos, and $\lambda(k, m)$ is the Fourier transform of the halo matter density profile, which we have assumed to be spherically symmetric and normalized such that the integral of the matter density profile $\rho(r, m)$, over all space is unity, $4\pi \int {\rm d}r \; r^2 \rho(r, m) = 1$. The two-halo term is

$$P_{\rm 2H}(k) = \frac{1}{\rho_{\rm M}^2} P^{\rm lin}(k) \left[\int {\rm d}m \; m \frac{{\rm d}n}{{\rm d}m} \lambda(k, m) b_{\rm h}(m) \right]^2, \quad (7)$$

where $P^{\rm lin}(k)$ is the matter power spectrum given by linear perturbation theory and $b_{\rm h}(m)$ is the mass-dependent halo bias. We calculate the linear matter power spectrum using the fitting formulae of Eisenstein and Hu [51] with the appropriate modifications for dark energy [52]. The halo model has known shortcomings (e.g., [53]), but we model the matter power spectrum in this way because it isolates the quantities we aim to study, namely the mean density profiles of halos of mass m, $\rho(r, m)$ and their Fourier transforms $\lambda(k, m)$.

Motivated by the findings of Ref. [28], we model the average mass density of halos using the density profile of Ref. [54],

$$\rho(r) \propto \frac{1}{(cr/R_{\rm 200m})(1 + cr/R_{\rm 200m})^2}, \quad (8)$$

truncated for $r > R_{200\mathrm{m}}$. The parameter c describes the relative concentration of mass toward the halo center. $R_{200\mathrm{m}}$ gives the extent of halo in the sense that the mass within $R_{200\mathrm{m}}$ is the halo mass m. We define halos as spherical objects within which the mean density is $200\rho_{\mathrm{M}}$, so that the mass and radius are related by $m = 4\pi(200\rho_{\mathrm{M}})R^3_{200\mathrm{m}}/3$. This convention is chosen to be consistent with the halo bias prescription that we use (see below). The density profile of Eq. (8) has a Fourier transform [48]

$$\begin{aligned}\lambda(k,c) \;=\; \frac{1}{f(c)}\Bigg\{ & \sin(\eta)[\mathrm{Si}([1+c]\eta) - \mathrm{Si}(\eta)] \\ & + \cos(\eta)[\mathrm{Ci}([1+c]\eta) - \mathrm{Ci}(\eta)] \\ & - \frac{\sin(\eta)}{[1+c]\eta}\Bigg\}, \end{aligned} \tag{9}$$

where $f(x) = \ln(1+x) - x/(1+x)$, $\eta = kR_{200\mathrm{m}}/c$, and $\mathrm{Si}(x)$ and $\mathrm{Ci}(x)$ are the sine and cosine integrals respectively.

In the case of dissipationless physics, we set the mean halo concentration as a function of mass and redshift according to a power law [55] (see also Refs. [56, 57, 58] and in particular Ref. [59] for a recent study of concentrations in the `Millennium Simulation` [85])

$$c^{\mathrm{STD}}(m,z) = 11[m/m_{\star,0}]^{-0.1}(1+z)^{-1} \tag{10}$$

where $m_{\star,0}$ is the mass of a typical object collapsing at $z = 0$ ($m_{\star,0} \simeq 2.2 \times 10^{12}\ h^{-1}\mathrm{M}_\odot$ in our fiducial cosmology, see below). The slight difference between Eq. (10) and the relation in Ref. [55] is due to the conversion between the the halo mass definition used in that study and the one we use [60]. Throughout this study we ignore the distribution in concentrations at fixed mass which is approximately log-normal [55]. For concentration distributions computed from N-body and hydrodynamic simulations, the relative influence of the spread in concentrations on convergence spectra is completely negligible on the scales we consider [61, 62]. For simplicity, we model the halo mass function and the halo bias using the relations of Ref. [63]. We reiterate here that when we refer to halo density profiles and halo concentration parameters, we mean the effective density profiles and concentrations of the composite systems of dark matter and baryons.

C. Fisher Matrix Analysis, Experimental Specifications, and Cosmological Parameters

We quantify the constraining power of observables using the Fisher information matrix. The Fisher matrix components are a sum over observables,

$$F_{\mathrm{ij}} = \sum_{\ell_{\mathrm{min}}}^{\ell_{\mathrm{max}}} (2\ell+1) f_{\mathrm{sky}} \sum_{\mathrm{A,B}} \frac{\partial \mathcal{O}_{\mathrm{A}}}{\partial p_{\mathrm{i}}} [C^{-1}]_{\mathrm{AB}} \frac{\partial \mathcal{O}_{\mathrm{B}}}{\partial p_{\mathrm{j}}} + F^{\mathrm{P}}_{\mathrm{ij}}, \tag{11}$$

where the $\mathcal{O}_{\mathrm{A}}$ represent the $N_{\mathrm{TOM}}(N_{\mathrm{TOM}}+1)/2$ observables of Eq. (1) and the index A runs over these observables, C_{AB} are the components of the covariance matrix of observables, and the p_{i} represent the parameters of the model. The sum over multipoles runs from some minimum multipole ℓ_{min} fixed by the sky coverage of the experiment. For simplicity, we set $\ell_{\mathrm{min}} = 2f_{\mathrm{sky}}^{-1/2}$, where f_{sky} is the fraction of the sky covered by the experiment; however, this choice is unimportant because constraints are dominated by considerably higher multipoles in all cases of interest. The multipole sum runs to some maximum multipole ℓ_{max}, which is typically fixed between $\ell_{\mathrm{max}} \sim 1000 - 3000$ so as to remain in the regime where several assumptions, including that of Gaussian statistics, are valid [61, 64, 65, 66, 67]. Furthermore, our modeling of baryonic effects is certainly not valid at significantly higher multipoles, so it is sensible to keep ℓ_{max} in this range for our purposes. We elaborate on this in section II D.

The inverse of the Fisher matrix approximates the parameter covariance locally about the maximum likelihood. As such, the measurement error of the ith parameter is $\sigma(p_{\mathrm{i}}) = [F^{-1}]_{\mathrm{ii}}$. The second term in Eq. (11) incorporates any Gaussian priors on the model parameters. In most of what follows, we assume modest priors on each parameter individually so that $F^{\mathrm{P}}_{\mathrm{ij}} = \delta_{\mathrm{ij}}/\sigma^2_{\mathrm{i}}$, where δ_{ij} is the Kronecker δ symbol. We discuss our parameters and priors in more detail below.

The Fisher matrix formalism also provides an estimate of parameter biases due to unknown systematic offsets in observables. Let $\mathcal{O}^{\mathrm{bias}}_{\mathrm{A}}$ be the difference between the true observable and the perturbed observable due to some systematic effect. In the limit of small systematic offsets, the parameters extracted from this set of observables will be biased by

$$\delta p_{\mathrm{i}} = \sum_{\mathrm{j}} [F^{-1}]_{\mathrm{ij}} \sum_{\ell} (2\ell+1) f_{\mathrm{sky}} \sum_{\mathrm{A,B}} \mathcal{O}^{\mathrm{bias}}_{\mathrm{A}} [C^{-1}]_{\mathrm{AB}} \frac{\partial \mathcal{O}_{\mathrm{B}}}{\partial p_{\mathrm{j}}}. \tag{12}$$

Observed spectra contain both a term due to signal and a noise term,

$$\bar{P}^{\mathrm{ij}}_{\kappa}(\ell) = P^{\mathrm{ij}}_{\kappa}(\ell) + n_{\mathrm{i}}\delta_{\mathrm{ij}}\langle\gamma^2\rangle, \tag{13}$$

where $\langle\gamma^2\rangle$ is the intrinsic source galaxy shape noise, and n_{i} is the surface density of sources in the ith tomographic bin and can be obtained by integrating Eq. (3) over all redshifts. The covariance between observables $\bar{P}^{\mathrm{ij}}_{\kappa}$ and $\bar{P}^{\mathrm{kl}}_{\kappa}$ is

$$C_{\mathrm{AB}} = \bar{P}^{\mathrm{ik}}_{\kappa}\bar{P}^{\mathrm{jl}}_{\kappa} + \bar{P}^{\mathrm{il}}_{\kappa}\bar{P}^{\mathrm{jk}}_{\kappa}, \tag{14}$$

where the i and j map to the observable index A, k and l map to B, and we have assumed the statistics of the convergence field to be Gaussian. We fix $\sqrt{\langle\gamma^2\rangle} = 0.2$ and study constraints from several forthcoming surveys defined by the parameters f_{sky} and $\bar{n}$, the total effective surface density of source galaxies on the sky. For

specificity, we study the limits expected from an experiment like the Dark Energy Survey (DES)[86] with $f_{\rm sky} = 0.12$ and $\bar{n} = 15/\mathrm{arcmin}^2$, a future space-based mission like the SuperNova/Acceleration Probe (SNAP)[87] with $f_{\rm sky} = 0.025$ and $\bar{n} = 100/\mathrm{arcmin}^2$, and a future ground-based survey like the Large Synoptic Survey Telescope (LSST)[88] with $f_{\rm sky} = 0.5$ and $\bar{n} = 50/\mathrm{arcmin}^2$.

We consider cosmologies defined by seven parameters. Three of these parameters describe the dark energy. The other four parameters and the values they take in our fiducial cosmological model are the total matter density $\omega_{\rm M} = \Omega_{\rm M} h^2 = 0.128$, the baryon density $\omega_{\rm B} = 0.0223$, the amplitude of curvature fluctuations at $k = 0.05$ Mpc^{-1} $\Delta^2_{\mathcal{R}} = 2.04 \times 10^{-9}$ (we actually vary $\ln \Delta^2_{\mathcal{R}}$), and the power-law index of the primordial power spectrum $n_{\rm s} = 0.958$. This fiducial model is motivated by the Wilkinson Microwave Anisotropy Probe three-year results [6]. We take very modest priors on these four parameters, $\sigma(\omega_{\rm M}) = 0.007$, $\sigma(\omega_{\rm B}) = 1.2 \times 10^{-3}$, $\sigma(\ln \Delta^2_{\mathcal{R}}) = 0.1$, and $\sigma(n_{\rm s}) = 0.05$, which are comparable to contemporary constraints (e.g., Refs. [6, 7]). We describe the dark energy by its present energy density parameter $\Omega_{\rm DE} = 0.76$, and an equation of state parameter that varies with scale factor as $w(a) = w_0 + (1-a)w_{\rm a}$. In our fiducial model, $w_0 = -1$ and $w_{\rm a} = 0$ and we assume no prior information on any dark energy parameter. As a reference, our fiducial model implies that the root-mean-square matter density fluctuations on a scale of $8\ h^{-1}$Mpc is $\sigma_8 \simeq 0.76$.

In addition to the marginalized errors in the cosmological parameters, we also quantify the constraining power of surveys by the figure of merit advocated in the report of the Dark Energy Task Force [41] (see Ref. [68] for a similar suggestion). The DETF figure of merit is the inverse of the area of the marginalized 95% ellipse in the $w_{\rm a}$-w_0 plane divided by π. Letting a and b denote the lengths of the principal axes of this ellipse, the figure of merit is $\mathcal{F} = 1/ab$. Many studies also quote a pivot scale factor $a_{\rm p}$, and a pivot value of the dark energy equation of state parameter $w_{\rm p} = w(a_{\rm p})$ [41, 68, 69]. The pivot scale factor is the scale factor at which the uncertainty in $w(a)$ is minimized, and is given by

$$a_{\rm p} = 1 + \frac{[F^{-1}]_{w_0 w_{\rm a}}}{[F^{-1}]_{w_{\rm a} w_{\rm a}}}. \tag{15}$$

The pivot equation of state parameter is simply

$$w_{\rm p} = w_0 + (1 - a_{\rm p}) w_{\rm a}. \tag{16}$$

Taking $w_{\rm a}$ along with $w_{\rm p}$ as the parameters describing the dark energy equation of state is convenient because the principal axes of the error ellipse lie along these coordinates. Moreover, the transformation is linear and preserves the area of the ellipse. In terms of the components of the Fisher matrix [Eq. (11)], the variance in $w_{\rm p}$ is given by

$$\sigma^2(w_{\rm p}) = [F^{-1}]_{w_0 w_0} - \frac{[F^{-1}]^2_{w_0 w_{\rm a}}}{[F^{-1}]_{w_{\rm a} w_{\rm a}}}. \tag{17}$$

The 95% confidence level in two dimensions occurs at $\simeq 2.48\sigma$, so that the area of the 95% ellipse is $\mathcal{A} \simeq 6.17\pi\sigma(w_{\rm a})\sigma(w_{\rm p})$. The DETF also quote values of $[\sigma(w_{\rm a})\sigma(w_{\rm p})]^{-1}$ in their summary tables [41]. Clearly, our figure of merit $\mathcal{F}$, is related to the numerical values quoted in the tables of the DETF report $[\sigma(w_{\rm p})\sigma(w_{\rm a})]^{-1}$, by

$$\mathcal{F} \simeq \frac{0.162}{\sigma(w_{\rm p})\sigma(w_{\rm a})}. \tag{18}$$

We intend to focus on the relative scaling of the figure of merit, so the details of the constants of proportionality here are of minimal importance.

D. Modeling the Effects of Baryons with Modified Halo Concentrations

Rudd et al. [28] demonstrated that the influence of baryons on the matter power spectrum is primarily due to the modified structure of individual dark matter halos. In fact, the modification is simple. Rudd et al. [28] found that the halos in their hydrodynamic simulations followed a concentration-mass relation that was significantly different from the relation derived from N-body simulations [e.g., Eq. (10)]. Rudd et al. [28] found that the description of halo structure as NFW halos with boosted concentrations was valid for halo-centric radii greater than approximately $0.04 R_{\rm 200m}$ [89]. Upon accounting for this difference, these authors found that they could model convergence power spectra derived from their simulations accurately out to multipoles as high as $\ell \sim 6000$. However, as noted in both Ref. [27] and Ref. [28], hydrodynamic simulations are not yet up to the task of providing accurate predictions for the properties of galaxies. So, while the net effect of galaxy formation on the power spectra may be well described by a modified, effective $c(m,z)$ relation, this effective $c(m,z)$ relation is not known. Consequently, it seems natural to calibrate the effective concentration-mass relation within the observational data itself and we explore several parameterizations of varying complexity for this relation. In the following section, we present results where both cosmology and the parameters of the $c(m,z)$ relation are determined simultaneously from observational data.

Neglecting baryonic physics, the relation between concentration and mass is known to be well characterized by a power law [Eq. (10), see Ref. [55, 59]]. Consequently, it seems natural to study power-law relations of the form

$$c(m,z) = c_0 [m/m_{\star,0}]^{\alpha} (1+z)^{-\beta}. \tag{19}$$

Further, it is reasonable to suppose that the redshift dependence is not modified from the standard N-body relation [Eq. (10)] because the majority of baryonic condensation is thought to have occurred at $z \gtrsim 1$ and because the redshift scaling in the standard case arises simply because virial radii grow as $R_{\rm 200m} \propto (1+z)^{-1}$ in

the absence of accretion. This scaling arises because halos are typically defined as an overdensity with respect to the mean density and the mean density dilutes as $\rho_{\rm M}\ (1+z)^{-3}$ while the structure of the bound object remains unchanged. We expect this second feature to be unmodified when including baryonic physics. Nevertheless, we study concentration relations of this form both with the redshift dependence fixed to $\beta = 1$ and with β free. We choose a fiducial concentration relation that is enhanced so that $c_0 = 15$ and $\alpha = -0.1$. This represents a 36% enhancement in halo concentrations while Rudd et al. [28] report a slightly larger enhancement in concentrations in their `DMG_SF` simulation for halos near m a few $\times 10^{14}\ h^{-1}{\rm M}_\odot$. As we demonstrate in Section III, it is the halos in this mass range that most influence convergence power spectra. We choose an enhancement slightly below the most relevant result from Ref. [28] because the simulation results likely overestimate the effective concentrations due to the well-documented overcooling problem of contemporary hydrodynamic simulations [70, 71, 72, 73, 74, 75, 76].

Though concentration relations normalized at $m = m_{\star,0}$ and redshift $z = 0$ are conventional in the literature on halo structure, this is likely not to be the most appropriate representation in the present context. Halos near $m \sim 10^{14}\ h^{-1}{\rm M}_\odot$ make the largest contribution to convergence power spectra [26, 77], and lensing weights are considerable at redshifts between $0.2 \lesssim z \lesssim 1$, so it is natural to suppose that lensing will be most sensitive to the structure of $\sim 10^{14}\ h^{-1}{\rm M}_\odot$ halos in a broad range of redshifts. In analogy with the the pivot scale factor and pivot equation of state parameter described in Section II C for the dark energy, we may define a pivot redshift $z_{\rm piv}$, and pivot mass $m_{\rm piv}$, for the $c(m,z)$ relation. We set the $z_{\rm piv}$ and $m_{\rm piv}$ as the redshift and mass at which the fractional uncertainty $\sigma(c)/c$ is minimized. The pivot concentration is $c_{\rm piv} = c(m_{\rm piv}, z_{\rm piv})$. The fractional uncertainty at the pivot concentration is

$$\begin{aligned}\frac{\sigma^2(c_{\rm piv})}{c_{\rm piv}^2} &= \frac{[F^{-1}]_{c_0c_0}}{c_0^2} + \ln^2(m_{\rm piv}/m_{\star,0})[F^{-1}]_{\alpha\alpha} \\ &+ \ln^2(1+z_{\rm piv})[F^{-1}]_{\beta\beta} \\ &+ \frac{2\ln(m_{\rm piv}/m_{\star,0})}{c_0}[F^{-1}]_{c_0\alpha} \\ &- \frac{2\ln(1+z_{\rm piv})}{c_0}[F^{-1}]_{c_0\beta} \\ &- 2\ln(m_{\rm piv}/m_{\star,0})\ln(1+z_{\rm piv})[F^{-1}]_{\alpha\beta}. \quad (20)\end{aligned}$$

The pivot redshift is

$$\ln(1+z_{\rm piv}) = \frac{1}{c_0}\frac{[F^{-1}]_{\alpha\alpha}[F^{-1}]_{c_0\beta} - [F^{-1}]_{c_0\alpha}[F^{-1}]_{\alpha\beta}}{[F^{-1}]_{\alpha\alpha}[F^{-1}]_{\beta\beta} - [F^{-1}]^2_{\alpha\beta}} \quad (21)$$

and the pivot mass is

$$\ln(m_{\rm piv}/m_{\star,0}) = \frac{1}{c_0}\frac{[F^{-1}]_{\beta\beta}[F^{-1}]_{c_0\alpha} - [F^{-1}]_{c_0\beta}[F^{-1}]_{\alpha\beta}}{[F^{-1}]^2_{\alpha\beta} - [F^{-1}]_{\alpha\alpha}[F^{-1}]_{\beta\beta}}. \quad (22)$$

In the following sections, we will quote pivot masses and redshifts and errors in $c_{\rm piv}$.

The $c(m,z)$ relation of Eq. (19) may be general enough to encompass most plausible behavior, particularly because the convergence spectra are most sensitive to a narrow range of halo masses near $m \sim 10^{14}\ h^{-1}{\rm M}_\odot$ for $\ell \sim 10^3$ [26, 77] (also see Sec. III). However, it is not unreasonable to suspect more complicated behavior. For example, the mass-to-light ratios of galaxy, group, and cluster halos are known to vary in a non-monotonic fashion with total mass (e.g., Ref. [78, 79, 80]) with a minimum near $m \sim 10^{11.5}\ h^{-1}{\rm M}_\odot$. As this minimum reflects some maximum efficiency for galaxy formation, it is natural to suspect that the relative boost in halo concentrations peaks at this halo mass and declines on either side of it. To hedge against the possibility of more complicated behavior than that in Eq. (19), we also explore a concentration relation with significantly more freedom.

In this more general relation we define values of concentration at $N_{\rm c}$ values of $\log(m/\ h^{-1}{\rm M}_\odot)$ evenly spaced in the log of the halo mass between $11 \le \log(m/\ h^{-1}{\rm M}_\odot) \le 16$. We have verified that extending this range to lower or higher masses has little effect as these masses contribute too little to the convergence spectra on scales of interest [26, 77]. The concentration values specify the mean halo concentration at the center of each mass bin and we spline interpolate between these values to enforce smoothness in the relation. This choice reflects our prejudice that the average concentration should always be a very smooth function of mass. In addition, we expect that at very high masses and very low masses baryonic condensation and galaxy formation should be inefficient, so we require that the standard relation [Eq. (10)] be recovered for masses $\log(m/\ h^{-1}{\rm M}_\odot) < 9$ and $\log(m/\ h^{-1}{\rm M}_\odot) > 18$. We enforce this by matching the spline onto the standard relation at these endpoints. In practice, the choice of boundary condition for the $c(m,z)$ at low and high masses is unimportant. We refer to our parameter set by subscripting a "c" with the logarithm of the mass at which this concentration is specified. For example, in a model with $N_{\rm c} = 5$, our concentration parameters are $c_{11.5}$, $c_{12.5}$, $c_{13.5}$, $c_{14.5}$, and $c_{15.5}$. We implement a variable redshift dependence as $c(m,z) = c(m,z=0)/(1+z)^\beta$.

To give the reader a sense of the influence of these changes on observables, we show the relative differences in the observable convergence spectra in Figure 1. For concreteness, we plot spectra in the power law $c(m,z)$ model with $c_0 = 15$ compared to the spectra computed using the standard relation of Eq. (10) derived from dissipationless simulations. We have used a model with five tomographic redshift bins, but for the sake of clarity we plot only three observables. These correspond to the spectra of the second and third tomographic bins and the cross spectrum between these bins. As a reminder, the *photometric* redshift limits of the second and third bins are $0.6 < z_{\rm p} \le 1.2$ and $1.2 < z_{\rm p} \le 1.8$ respectively. As one would expect, any effect on concentrations becomes quite large at $\ell \gtrsim 10^3$. However, it is worth noting

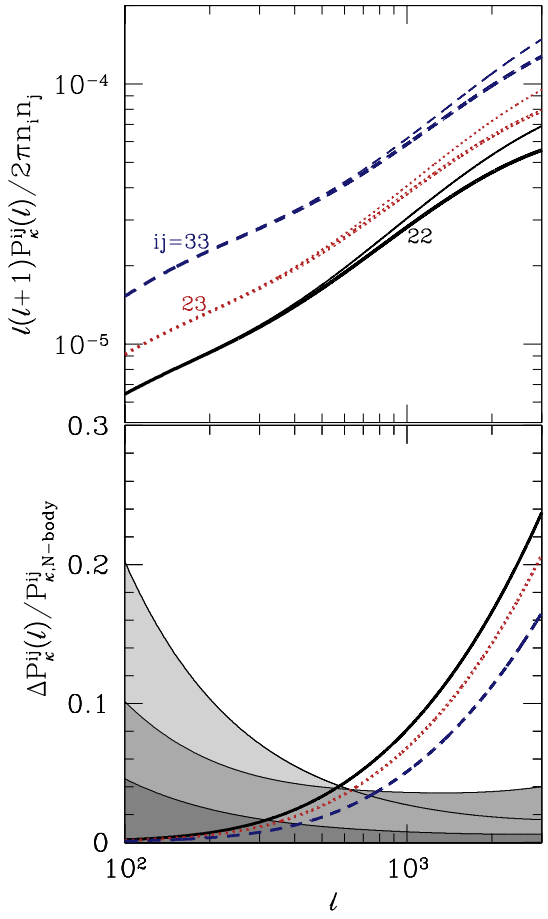

FIG. 1: The differences in convergence spectra for the fiducial model of boosted power-law concentrations (*thin lines*) relative to the standard case with concentrations derived from dissipationless simulations (*thick lines*). In the top panel we show the power spectra explicitly and in the bottom panel we show the change in observables scaled to the standard N-body concentration case. We use five tomographic bins throughout most of this work and we have dropped the number weighting of spectra for the purposes of this demonstration only. For simplicity we show only the behavior of three observables, the spectra in the second and third redshift bins P^{22}_{κ}/n_2^2 and P^{33}_{κ}/n_3^2, and the cross spectrum $P^{23}_{\kappa}/n_2 n_3$. The behavior of other observables is qualitatively similar. The shaded bands show, from outermost to the innermost at left, the variance in P^{33}_{κ} for SNAP, DES, and LSST in bands of width $\Delta\ell/\ell = 1/10$. Note that the sensitivity of SNAP overtakes that of DES by $\ell \sim 600$ as SNAP is far deeper than DES. We show this by extending the upper limit of the shaded SNAP band as a solid line below the filled DES region.

that the effect is not negligible even at much lower multipoles and that all of the experiments we consider would be sensitive to such effects even at multipoles as low as several hundred.

III. RESULTS

A. Dark Energy Constraints and Parameter Biases

We begin our presentation of results with parameter constraints in the standard case of no modifications to halo structure from baryonic processes. This case corresponds to perfect knowledge of halo density profiles and has been considered numerous times in the literature already. We include this partly to give a frame of reference for the results that follow. More importantly, we show dark energy parameter constraints as a function of the maximum multipole $\ell_{\rm max}$ used in the sum in Eq. (11) so that one can compare the relative merits of marginalizing over an unknown halo concentration-mass relation with simply ignoring the high multipole moments where baryonic effects are most severe. Throughout this section, we label the uncertainties in parameter p obtained by including multipoles out to $\ell_{\rm max} = \ell$ as $\sigma_\ell(p)$.

Constraints on dark energy parameters in the absence of any unknown baryonic processes as a function of $\ell_{\rm max}$ are shown in Figure 2, where we have taken $N_{\rm TOM} = 5$ as prescribed by Ref. [42]. Unless otherwise noted, this choice pertains to all results on parameter constraints. With modest prior information, weak lensing tomography alone can constrain dark energy parameters very well. Using information out to an $\ell_{\rm max} = 3000$, the marginalized constraints from DES, SNAP, and LSST respectively are $\sigma^{\rm STD}_{3000}(\Omega_{\rm DE}) = 0.023, 0.018, 0.0066$, $\sigma^{\rm STD}_{3000}(w_0) = 0.26, 0.19, 0.069$, and $\sigma^{\rm STD}_{3000}(w_{\rm a}) = 0.74, 0.56, 0.21$. Constraints from LSST are the most stringent because the experiment combines extensive sky coverage with depth. SNAP and DES are comparable (considering *only* weak lensing information) over this range of scales. SNAP, being extraordinarily deep, can exploit information in very high multipoles while the constraints from DES overtake those from SNAP if only multipoles $\ell \lesssim 400$ are used because of its larger sky coverage. Hereafter, we plot our results including self-calibration of baryonic processes relative to these standard results which represent the limit of perfect knowledge of internal halo structure.

Both Jing et al. [27] and Rudd et al. [28] pointed out that the modifications of the convergence power spectra due to baryonic physics are likely to be large and to extend over a wide range of multipoles, but neither of these studies translated this systematic into its influence on cosmological parameter constraints. In particular, it is interesting to examine the bias in dark energy parameters if baryonic physics are neglected. If the bias is small compared to the statistical uncertainties in Fig. 2, then it need not be a major concern because it is unlikely to lead to rejection of the true cosmology based on these data.

We show the biases in the inferred values of w_0 and $w_{\rm a}$ as a function of $\ell_{\rm max}$ in units of their uncertainties in Figure 3. To compute the biases shown in Fig. 3, we assumed the true power spectra to be given by the

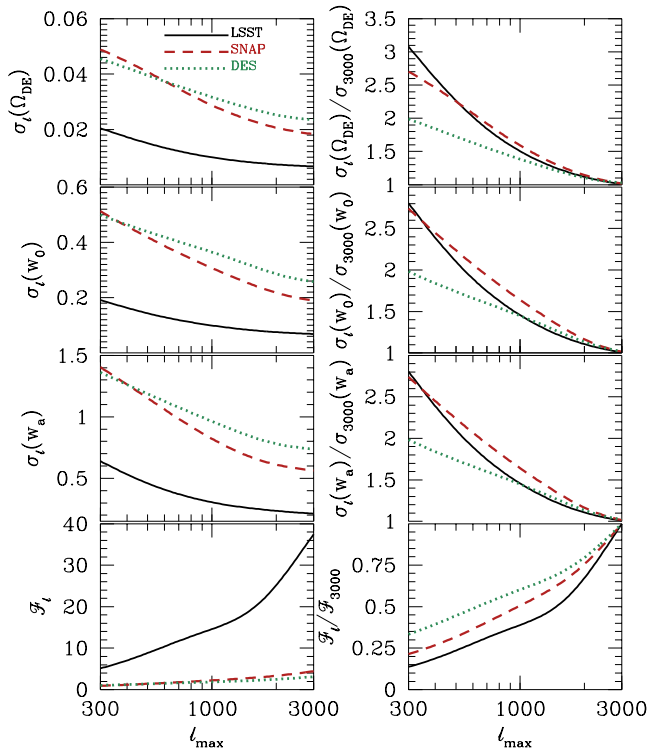

FIG. 2: Standard marginalized dark energy parameter constraints as a function of maximum multipole $\ell_{\rm max}$. The left panels show the 1σ uncertainties in the three dark energy parameters $\Omega_{\rm DE}$, w_0, and $w_{\rm a}$ from the top down. The bottom panel shows the dark energy figure of merit $\mathcal{F}$ as a function of maximum multipole. The *solid* line corresponds to an LSST-like experiment, the *dashed* line corresponds to a SNAP-like experiment, and the *dotted* line corresponds to an experiment similar to DES. The right panels show the same quantities scaled by the uncertainties obtained at $\ell_{\rm max} = 3000$ in order to show the relative scaling of dark energy constraints with $\ell_{\rm max}$ more clearly.

fiducial power-law concentration model with $c_0 = 15$, which is a $\sim 36\%$ enhancement relative to the standard concentration-mass relation, and employed the approximation of Eq. (12). The magnitudes of the biases show sharp minima in many cases. These represent changes in the signs of the biases. Generally, $\delta(w_0) > 0$ and $\delta(w_{\rm a}) < 0$ at the lowest multipoles. Note that in all cases biases become large compared to the uncertainties in the parameters, so the approximation used to compute them breaks down. These large biases are unlikely to be the product of any analysis. Rather the team performing the analysis would notice something amiss because the best-fitting models would be relatively poor fits to the data and this would be evident in some criterion used to assess fit quality, such as the χ^2 per degree of freedom.

The details of the parameter biases are a strong function of the choice of fiducial cosmology. This is because both the signal-to-noise ratios and the scales at which nonlinear effects become important are strong functions of the fiducial model. We illustrate this in Fig. 3 by showing biases computed about the fiducial cosmological model of Ma et al. [42], which more closely resembles the cosmology from the Wilkinson Microwave Anisotropy Probe first year results [81]. The most important differences between our fiducial model and the fiducial model of Ma et al. [42] are that Ma et al. [42] took $n_{\rm s} = 1$ (compared to $n_{\rm s} = 0.958$) and a slightly higher power spectrum normalization, implying a larger mass variance on 8 h^{-1}Mpc scales of $\sigma_8 \simeq 0.9$. In the Ma et al. [42] fiducial model, parameter inferences are more sensitive to small systematics on quasi-linear and nonlinear scales for two reasons. First, the signal is relatively higher. Second, nonlinear effects become important on larger scales (smaller ℓ) in models with more power. Both of these effects are reflected in Fig. 3. Near the Ma et al. [42] fiducial model with relatively greater power, biases are typically larger and they become important at smaller wavenumbers. Throughout the remainder of this section, we give our primary results derived about the fiducial model of Section II C; however, we often compare these to results derived about the fiducial model of Ma et al. [42] in order to indicate the importance of the choice of fiducial model.

As the details of the fiducial model have a significant influence on parameter biases and the linearized relation of Eq. (12) should break down for biases large compared to their uncertainties, it is hard to make concrete statements about parameter biases. Nevertheless, Fig. 3 is an indicator that such biases may be significant, even at multipoles $\ell < 10^3$. LSST will provide the tightest constraints on dark energy parameters over this range of scales, primarily because it is extremely wide, yet this makes LSST most susceptible to unknown baryonic physics in a relative sense. In the absence of reliable and robust predictions for power spectra in the presence of baryons or any other method for dealing with the influence of baryonic processes, one could safely force the biases to be relatively small compared to the uncertainties by disregarding multipoles above some $\ell_{\rm max}$. This and more elaborate strategies for removing some of the small-scale information in weak lensing tomography have been studied by Huterer and White [82]. Fig. 3 suggests that this would require setting $\ell_{\rm max}$ to no greater than many hundreds, though the details depend upon both the experiment (they are most stringent for LSST) and the underlying cosmology. Comparing with Fig. 2, this corresponds to a degradation of dark energy parameter constraints by a factor of $\sim 2-3$ or more relative to the constraints achieved by setting $\ell_{\rm max} = 3000$ in the standard case of perfect knowledge of halo density profiles. Correspondingly, the decrease in the DETF figure of merit is approximately a factor of $\sim 4-7$. We note that these effects are more important in models with more small-scale power, so that about a cosmology with a higher value of $\sigma_8 \simeq 0.9$, dark energy parameter constraints can be degraded by more than a factor of three and the figure of merit can be decreased by nearly a factor of ten. In what

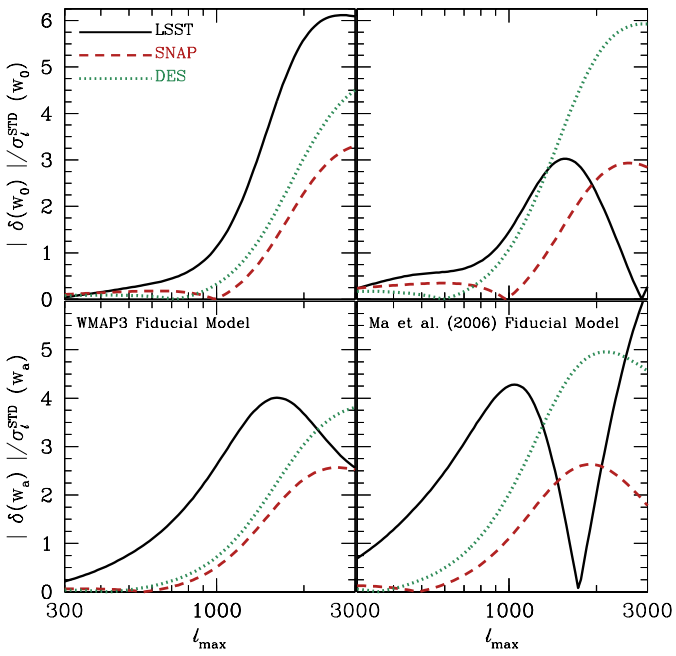

FIG. 3: Biases in inferred dark energy parameters due the ignorance of baryonic physics. We show biases by assuming the true model to have a power-law concentration-mass relation with $c_0 = 15$ instead of $c_0 = 11$ as in the case of models that neglect baryonic physics. Results for DES, SNAP, and LSST are shown as labeled in the upper left portion of the figure. In all cases, we show bias relative to the 1σ measurement uncertainty in the relevant parameter. The top panels show the biases for w_0 and the bottom panels show the biases for w_a. Notice that we show biases about both the fiducial model that we use in this work (*left column*) and the model of Ma et al. [42] which has significantly more small-scale power ($\sigma_8 \simeq 0.9$, *right column*). The minima in the magnitudes of the biases reflect changes in sign. Generally $\delta(w_0) > 0$ at the lowest multipoles and $\delta(w_a) < 0$ at the lowest multipoles. In the case of LSST, the first change in sign in $\delta(w_0)$ occurs at $\ell_{max} < 300$, so that $\delta(w_0) < 0$ at $\ell_{max} = 300$. The approximations used to compute the parameter bias [see Eq. (12)] break down in all cases as the biases become larger than their uncertainties at high multipoles. These estimates indicate that the biases are likely to be non-negligible.

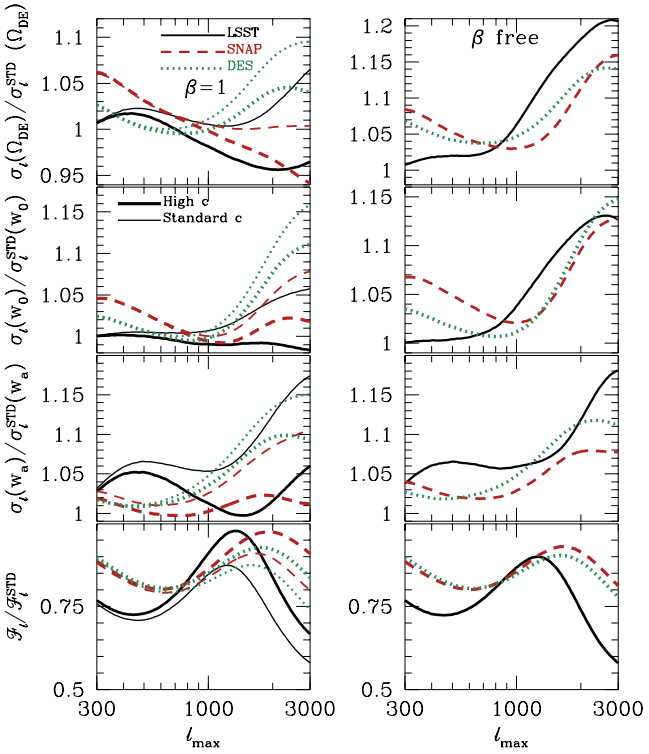

FIG. 4: The relative degradation in parameter constraints as a function of maximum multipole used to derive constraints for the case of a power-law concentration mass relation [Eq. (19)]. The vertical axes are the parameter constraints in the new concentration model divided by the constraints in the standard case. In the *left* panel, we show constraints in a model with fixed redshift dependence. The *thick* lines show constraints about a fiducial model with concentrations enhanced relative to the standard N-body case ($c_0 = 15$) while the *thin* lines show constraints about the N-body $c^{\rm STD}(m, z)$ ($c_0 = 11$) as fiducial model [Eq. (10)]. In the *right* panel we show constraints in a model in which the power-law index describing the redshift dependence of concentrations is variable. The fiducial model in this case and in all subsequent plots has enhanced halo concentrations relative to the dissipationless case. Note that the dynamic ranges on the vertical axes are different in the left and right panels. In all panels, the *solid* line represents LSST, the *dashed* line represents SNAP, and the *dotted* line represents DES.

follows, we show that internal self calibration of baryonic effects may be a viable alternative to this degradation in parameter constraints.

B. Dark Energy Constraint Degradation: Power-Law Halo Mass-Concentration Relations

We consider the degradation in parameter constraints sequentially from the power-law $c(m, z)$ model to the more general cases in order to give a sense of the gradual degradation from the additional degrees of freedom. The relative degradation in dark energy parameters in the power-law $c(m, z)$ models is shown in Figure 4. The left panel of Fig. 4 shows constraints with a fixed redshift dependence and the right panel shows constraints with a variable redshift dependence parameter β. This figure shows that the degradation of dark energy parameter constraints is relatively small and that it behooves one to model the unknown baryonic effects and continue to use high multipole moments rather than cut out information above some relatively low ℓ_{max}. Provided there is some compelling justification for these relatively restricted concentration models, we can eliminate the bias caused by unknown halo structure while dark energy con-

straints will be degraded by only $\sim 15-20\%$ or less in all cases. This cost is relatively low compared to the cost of using only multipoles below several hundred to constrain dark energy and, as we discuss below, the nuisance parameters of this analysis are physical parameters of interest in their own right.

Aside from this overriding point, there are several other features worthy of note. First, notice that there are instances (depending upon multipole range and experiment) in which the model with extra freedom provides better constraints than the standard model with known halo concentrations. This is due to our assumption that concentrations are enhanced (we take $c_0 = 15$ in our model with baryons compared to $c_0 = 11$ as given by N-body simulations) resulting in increased signal over a wide range of scales (See Fig. 1). The thin lines in the left panel of Fig. 4 show constraints about the standard $c(m,z)$ relation with $c_0 = 11$ as fiducial model. In this case, there is no boost in signal and the constraints are always poorer than in the model with perfect knowledge of $c(m,z)$, though not by much. Hereafter, we quote results for a fiducial model with enhanced halo concentrations relative to the standard N-body values. In all cases, the choice of fiducial cosmological parameters affects parameter constraints at levels similar to those shown in the left panel of Fig. 4.

In addition, observe that in the panels of Fig. 4 the relative degradation has a peak at multipoles of a few thousand with some variation depending upon the parameter of interest and the experiment. The peaks are more prominent in the right panels. In fact these features would also be apparent in the left panels of the figure, but are mostly omitted as they lie beyond our choice of $\ell_{\rm max} = 3000$. The origins of these features are simple to understand. The effect of concentrations is predominantly a high-ℓ phenomenon. As one approaches $\ell \sim 2000$ from the low multipole side, the unknown concentrations are degrading dark energy constraints rapidly because their effects are just beginning to appear and can at some level be mimicked by the dark energy parameters. However, as one continues to higher multipoles ($\ell \gtrsim 3 \times 10^3$), the concentration effects become increasingly distinguishable from those attributable to dark energy parameters, these degeneracies are broken and constraints improve to higher multipoles thereafter. The low-ℓ feature in these plots is due to a similar degeneracy primarily between the power-law index α and the dark energy equation of state parameters. Such features caused by the gradual elimination of degeneracies with the inclusion of information from ever higher multipoles are generic in the concentration models that we explore and are present in subsequent plots as well. In all cases, these "rolling hills" represent the sequential introduction and elimination of parameter degeneracies and we do not expound upon the details of each degenerate direction in this study in the interest of brevity.

It is important to stress that tomographic information is a crucial ingredient in minimizing parameter constraint

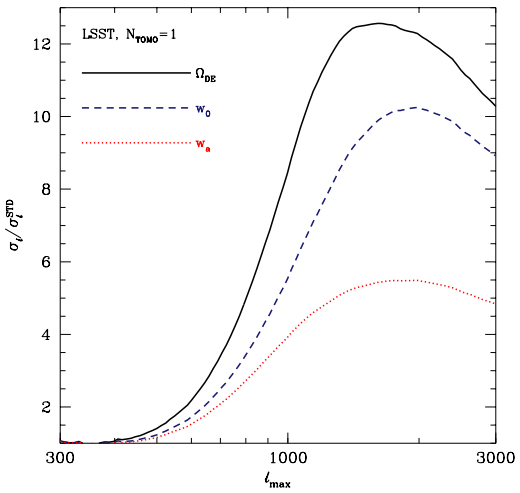

FIG. 5: The degradation in dark energy parameter constraints without tomographic information. This figure shows the relative errors compared to the case of perfect knowledge of effective halo concentrations as a function of $\ell_{\rm max}$ as in Fig. 4, but with no tomography. To illustrate this point, we use the power law $c(m,z)$ model with variable redshift index β. For the sake of clarity, we show only the case of LSST here, but the loss of constraining power is dramatic for all experiments.

degradation in the case of unknown halo concentrations. For example, eliminating tomographic information (setting $N_{\rm TOM} = 1$) dramatically reduces the ability of such surveys to calibrate for unknown halo concentrations. We find that in the case of the power-law class of concentration models with variable redshift index β, eliminating tomographic information in both the concentration-marginalized results and the N-body standard causes the relative degradation to rise from the $\sim 15\%$ level as shown in Fig. 4 to a factor of ~ 5 for $w_{\rm a}$ and a factor of ~ 10 for $\Omega_{\rm DE}$ and w_0. Note that this degradation is with respect to an already degraded baseline with no tomographic information. Figure 5 shows an example of the degradation in dark energy parameter constraints without tomography for the LSST experiment. Moreover, note that this level of dark energy information loss extends to multipoles as low as $\ell_{\rm max} \sim 600$. On the other hand, we find that constraints on dark energy parameters effectively saturate at $N_{\rm TOM} = 5$ getting only very gradually better with increasingly fine photometric redshift binning. For instance, increasing to $N_{\rm TOM} = 10$ only gives a few percent decrease in dark energy parameter errors.

The importance of tomographic information has both positive and negative aspects. On the negative side, it stresses the need for accurate photometric redshifts and photometric redshift distributions with well-understood properties. However, it suggests that the ability of future surveys to self calibrate does not rely solely on the

shapes of the power spectra produced by modified baryonic physics being non-degenerate with those arising due to dark energy effects. To be more specific, this also suggests that this success is not limited to very restrictive $c(m,z)$ prescriptions. For example, if the power spectra shapes obtained by modifying halo concentrations were in no way degenerate with the shapes obtained by varying dark energy parameters, eliminating tomographic information would not lead to further degradation in parameter constraints because even in this case the non-degenerate parameters could not compensate for each other. That constraints do significantly degrade in the case of no tomography suggests that dark energy and concentrations may lead to degenerate power spectra but that tomography helps distinguish the two. Tomographic information effectively provides several handles on the relative distances to the sources in the different photometric redshift bins [Eq. (2)] and enables one to distinguish between contributions to the shear from high redshift and low wavenumber from contributions at high wavenumber and low redshift, both of which may contribute at a single multipole. These internal consistency checks within weak lensing tomography render the dark energy and concentration parameters relatively distinguishable. Already, this suggests that the more general concentration relations we describe below will not lead to drastic dark energy parameter degradation.

C. Constraint Degradation: Binned Halo Mass-Concentration Relation

We now present parameter constraints in the context of our more general, binned $c(m,z)$ models. Based on the discussion of the previous section, there is cause to be optimistic that self calibration with a more general relation for halo concentrations will quite successful. Indeed, Figure 6 reveals this to be the case. Maximal parameter degradation is $\sim 30\%$ or less in all cases, so again self calibration performs better than the more drastic measure of disregarding the information contained in multipoles larger than a few hundred. Figure 6 depicts the case of a five-bin concentration-mass relation for concreteness; however, we have found that the level of degradation is relatively robust to the number of bins used. In fact, the level of degradation remains below a worst case degradation of 50% in $\Omega_{\rm DE}$ and $w_{\rm a}$ and 40% in w_0 for LSST and is below 40% in all parameters for DES and SNAP using 12 bins over the same mass range ($11 < \log(m/\ h^{-1}{\rm M}_\odot) < 16$). Given our prejudice that the concentration-mass relation should be a very smooth function of halo mass, this suggests that self calibration can successfully distinguish the variety of such relations realized in the universe while providing stringent constraints on dark energy.

The features in Fig. 6 are qualitatively similar to those in Fig. 4. The fact that there are multiple features in this case reflects the additional freedom in the concentration relation. Each concentration bin influences convergence spectra over a particular range of scales. The largest halos contribute on the largest scales, while the smaller halos become increasingly important with increasing multipole [26, 77]. In this case, the concentration parameters begin to be constrained gradually, from highest to lowest mass, as one increases $\ell_{\rm max}$. Aside from these features, the primary aim of Figure 6 is to illustrate the important, global point that dark energy parameter constraints are robust to very general concentration relations. Being the most sensitive instrument over the range of scales we consider, LSST is most sensitive to these effects, but even in this case the cost of avoiding the potential bias shown in Fig. 3 is low.

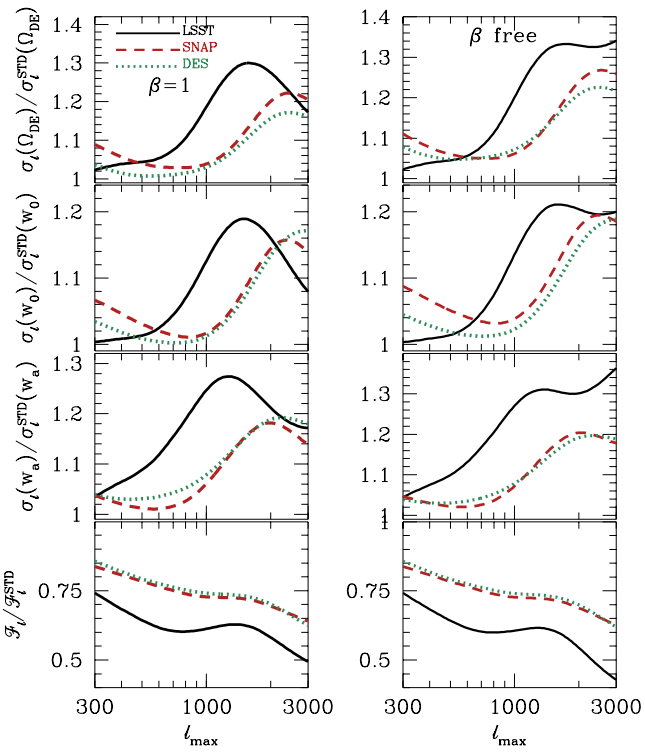

FIG. 6: The relative degradation in parameter constraints as a function of maximum multipole used to derive constraints for the case of the binned concentration mass relation. The vertical axes are the parameter constraints in the new concentration model divided by the constraints in the standard case. In the *left* panel, we show constraints in a model with fixed redshift dependence. In the *right* panel we show constraints in a model in which the power-law index describing concentration redshift dependence is variable. In all panels, the *solid* line represents LSST, the *dashed* line represents SNAP, and the *dotted* line represents DES.

D. Constraints on Concentrations from Weak Lensing Tomography

To this point, we have considered the unknown structure of halos to be a contaminant that degrades our ability to study the cosmic dark energy. However, observational constraints on concentrations are interesting in their own right. Indeed, we were driven to consider general parameterizations of halo structure because the baryonic physics that govern galaxy formation and influence the structures of halos is very uncertain. Direct constraints on concentrations may help to inform models of galaxy formation. Furthermore, constraints derived from a weak lensing survey as described above, would not be subject to the same selection as studies of galaxy groups and clusters or studies that rely on selecting sample members or stacking systems according to some member property. Therefore, these constraints can complement other techniques even if they are not directly competitive with other methods. We now focus on the constraints on halo concentrations that can be derived from weak lensing tomography.

Consider first constraints on the effective halo mass-concentration relation in the power-law concentration mass relation. Figure 7 shows two-dimensional confidence contours for the concentrations of halos after marginalizing over all other parameters, including dark energy. For convenience, the pivot masses and redshifts are listed in the upper right portion of this plot. Concentrations are very well determined near halo masses of $\sim 1 \times 10^{14}\ h^{-1}\mathrm{M}_\odot$ and a redshift $z \sim 0.2$. The slight differences in these values for each experiment reflect the fact that the statistical errors have a different scale dependence for each experiment. LSST has the greatest sky coverage, so the LSST pivot mass is the largest. Conversely, SNAP has much less sky coverage but with a galaxy number density of $\bar{n} = 100$ arcmin^{-2} it is very deep and has the smallest $m_{\rm piv}$. These $m_{\rm piv}$ and $z_{\rm piv}$ values are not unexpected. It is already well known that these masses are the largest contributors to the convergence power near $\ell \sim 10^3$ [26, 77].

The concentration constraints achieved in the course of this self calibration are stringent and potentially very useful. Marginalizing over the other parameters, LSST alone can provide a $\sim 5\%$ constraint on $c_{\rm piv}$ at 1σ, and can constrain the mass and redshift power-law indices to $\sigma(\alpha) = 0.08$ and $\sigma(\beta) = 0.27$ respectively. Both SNAP and DES constrain $c_{\rm piv}$ at the $\sim 10\%$ level.

Figure 8 shows concentration parameter constraints on the binned $c(m, z)$ relation model. First, recall that our convention is to designate our concentration parameters with a subscript of the value of the logarithm of the halo mass at the bin center. The parameter that describes halo concentrations at $m = 10^{13.5}\ h^{-1}\mathrm{M}_\odot$ is $c_{13.5}$ and so on. Rather than displaying all parameter constraints, Figure 8 shows a reduced set of parameters that are at least mildly constrained by the experiments that we consider. The other concentration parameters

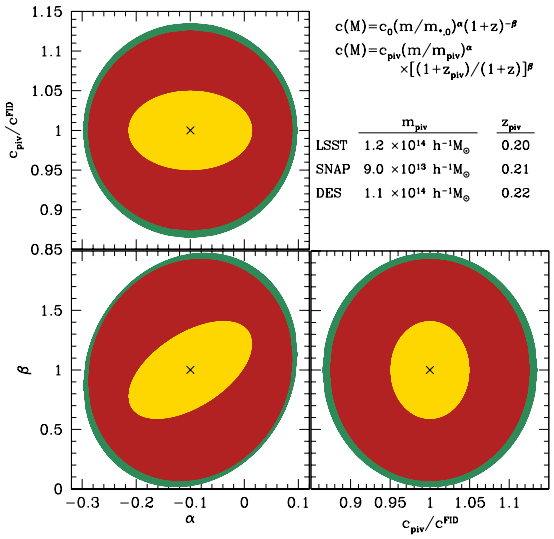

FIG. 7: Constraints on the effective halo concentration parameters from tomographic weak lensing after marginalizing over the uncertainty in cosmological parameters. This plot shows 1σ confidence contours on the parameters of the power-law concentration relation. We show the fractional uncertainty in $c_{\rm piv}$ relative to the fiducial model. Recall that the pivot concentration is the concentration at the halo mass and redshift at which concentrations are best determined. In all panels, from outermost to innermost, the contours correspond to those achievable with DES, SNAP, and LSST using multipoles up to $\ell_{\rm max} = 3000$. In the upper right portion of the plot, we list the parameterization and the values of the pivot masses and redshifts for convenience.

are constrained at uninteresting levels in all cases.

The fact that halo concentrations are most well constrained near halo masses near $\sim 10^{14}\ h^{-1}\mathrm{M}_\odot$ can be seen directly in Figure 8. This is clearly the most well constrained parameter. In fact, this parameter can be constrained with an uncertainty $\sigma(c_{14.5})/c_{14.5} = 0.48$ relative to the fiducial value by LSST alone. In the Ma et al. [42] fiducial model with greater small-scale power, LSST constrains this parameter relatively more stringently with $\sigma(c_{14.5})/c_{14.5} = 0.31$. Generally, this parameter is somewhat degenerate with the concentration value at the next lowest mass bin $c_{13.5}$, and a combination of these two parameters is constrained at interesting levels. As with the power-law case, the redshift dependence is comparably poorly constrained.

Though the constraints presented in Fig. 8 are modest, those in the power-law model of Fig. 7 are encouraging and recall that we have been rather conservative in our priors. Given that precise concentration constraints may inform the modeling of baryonic physics, it is interesting to estimate the best possible constraints on concentrations that may be achieved with these methods. To minimize the interplay between dark energy and concentration parameters, we may assume that dark energy parameters are known extremely well from other experi-

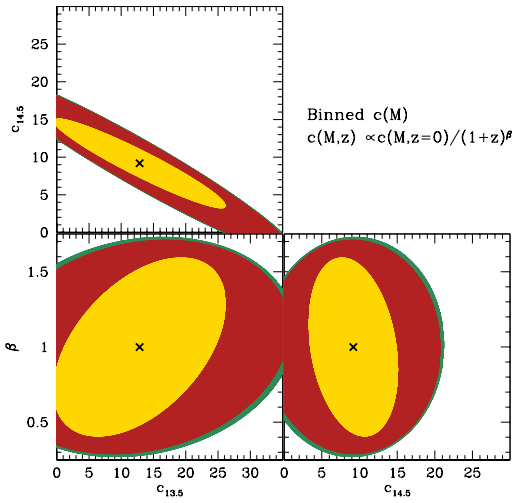

FIG. 8: Constraints on the effective halo concentration parameters from tomographic weak lensing after marginalizing over the uncertainty in cosmological parameters. We show the usefully constrained combination of parameters in the $c_{13.5}$-$c_{14.5}$ plane and projections of these parameters with the redshift variable β. In all panels, from outermost to innermost, the contours correspond to the 1σ contours achievable with DES, SNAP, and LSST with $\ell_{\rm max} = 3000$.

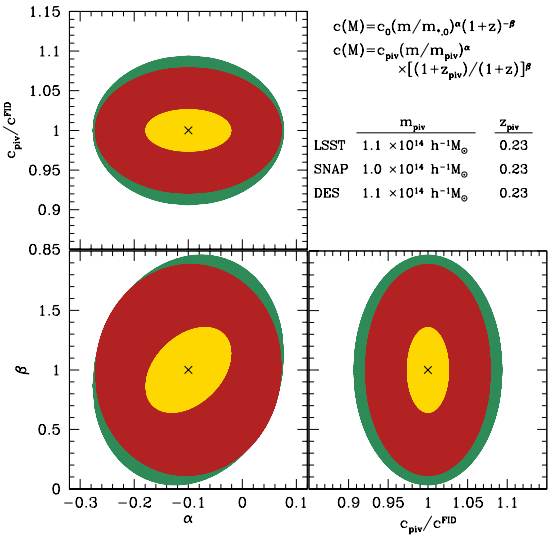

FIG. 9: Same as Figure 7, but assuming prior constraints on cosmological parameters at levels that are expected from a combination of the Planck cosmic microwave background satellite and supernovae luminosity distance measures from SNAP. The additional prior matrix for this analysis is from Ref. [83].

ments, for example through the supernovae measured by SNAP itself, and that we aim to measure effective halo concentrations via weak lensing. This is analogous to the dark energy constraints shown in Fig. 2, where it was assumed that concentrations were known perfectly, but in this case it is the cosmology that we assume to be well constrained.

To estimate concentration constraints in this scenario realistically, we assume that we have prior knowledge of cosmological parameters that exceed the contemporary priors that we have thus far assumed. To be specific, we add priors that are characteristic of projected constraints from the Planck cosmic microwave background mission and the supernova luminosity distance component of SNAP. In this case, the prior matrix does not have the simple diagonal form of our previous prior matrices. We have taken the prior Fisher matrices from the analysis of SNAP and Planck constraints in [83].

We show constraints on effective halo concentrations in the power-law concentration model assuming much more restrictive priors on cosmological parameters in Figure 9. First, note the slight changes in the pivot masses and pivot redshifts. More importantly, reducing the dark energy degrees of freedom significantly tightens constraints on effective halo concentrations. For example, the 1σ LSST constraint on $c_{\rm piv}$ drops to about $\sim 2\%$. Meanwhile, the LSST constraints on the mass dependent power-law index becomes $\sigma(\alpha) \simeq 0.04$. Restricting the space of cosmological parameters results in marginal improvement on the redshift index, with $\sigma(\beta) \simeq 0.24$. Both SNAP and DES also constrain concentrations stringently near the pivot mass and redshift, giving 1σ constraints at the $\sim 5\%$ and $\sim 7\%$ levels respectively.

The improvements with better cosmology priors are also noteworthy in the case of the general, binned $c(m, z)$ relation. We show constraints on the subset of most well constrained parameters in Figure 10. Consider the case of the LSST experiment, for which the constraints are the most stringent. In this case, the most significant improvement is realized for the redshift index β, with $\sigma(\beta) = 0.3$, while the constraint on $c_{13.5}$ decreases to just under 50%. The constraint on the concentration parameter $c_{14.5}$ from LSST drops to rather meaningful levels with $\sigma(c_{14.5})/c_{14.5} \simeq 0.3$. Constraints in this regime are particularly sensitive to the true cosmology, which sets the signal-to-noise level of the forthcoming measurements. In the Ma et al. [42] fiducial model with $\sigma_8 \simeq 0.9$, the parameters $c_{14.5}$ and $c_{13.5}$ can be independently constrained to within 21% and 34% respectively with LSST.

E. Constraint Degradation with Prior Knowledge of Halo Concentrations

The experiments we have considered will report results beginning in the year 2011 in the earliest case of the DES or later. Of course, it is hard to predict the pace of theoretical and observational studies of halo concentrations, but it seems reasonable to assume that over the next decade there will be some, perhaps significant, improvement and that this progress will be able to inform the

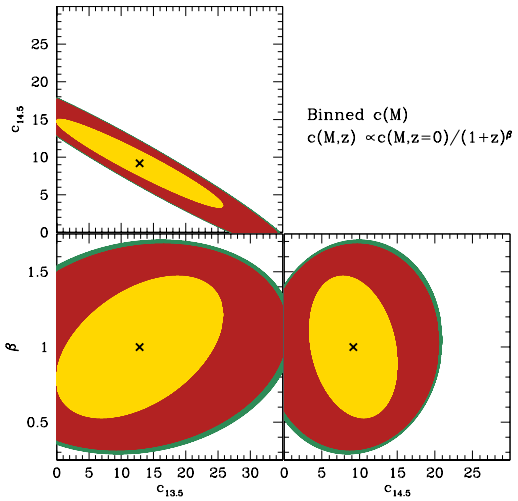

FIG. 10: Same as Figure 8, but assuming assuming prior constraints on cosmological parameters at levels expected from a combination of the Planck cosmic microwave background satellite and supernovae luminosity distance measures from SNAP. The additional priors for this analysis are from Ref. [83].

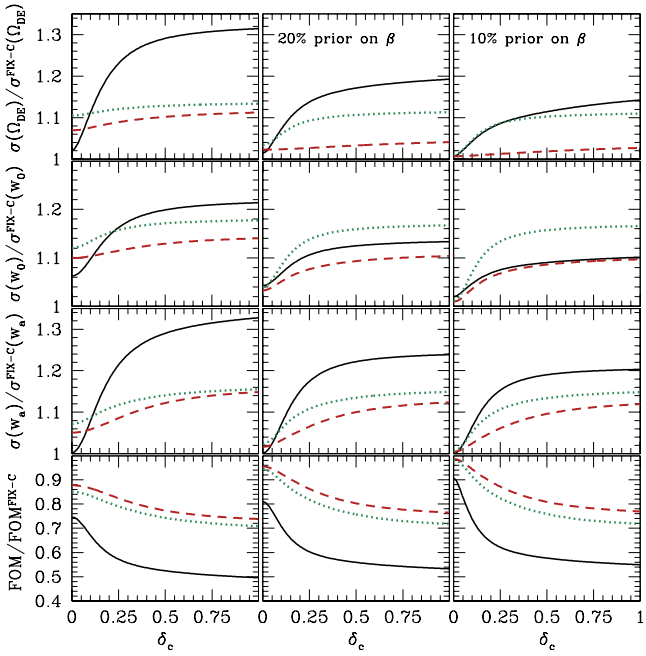

FIG. 11: The dependence of dark energy constraints on priors on the $c(m,z)$ relation. We plot the uncertainties in each parameter, scaled by the uncertainty under the assumption of perfect knowledge of the concentrations of halos $\sigma^{\rm FIX-C}$, as a function of the fractional prior on the amplitude of concentrations $\delta_{\rm c}$. As in Fig. 2, the rows from top to bottom show constraints on $\Omega_{\rm DE}$, w_0, and $w_{\rm a}$, while the bottom panels show the dark energy figure of merit, $\mathcal{F}$. The leftmost column shows constraints with no prior on β, the middle column shows constraints with a 20% prior on β, and the rightmost column shows constraints with a 10% prior on β. The line types are as in Fig. 2, namely, the *solid* line gives results for LSST, the *dashed* line corresponds to SNAP weak lensing, and the *dotted* line corresponds to DES.

actual analysis of future weak lensing data. As such, it is interesting to explore the way in which prior constraints on the $c(m,z)$ relation influence dark energy parameter degradation from tomographic weak lensing.

In this section, we consider the influence of priors in the case of the binned $c(m,z)$ relation. For simplicity, we assume that the concentrations in all mass bins, $c_{11.5}$ through $c_{15.5}$, have a prior constraint of some fraction of their fiducial value. Let us designate this fraction $\delta_{\rm c}$. We illustrate the effects of prior knowledge of the $c(m,z)$ relation on parameter constraints by computing the parameter uncertainties using all information out to a maximum multipole $\ell_{\rm max} = 3000$ as a function of prior $\delta_{\rm c}$. Though we take a single parameter to describe the prior in the interest of simplicity, it is clearly the prior on the parameter $c_{14.5}$ that is most important (see Sec. III D). We present results scaled relative to the uncertainties that would be derived under the assumption of perfect knowledge of effective halo concentrations, $\sigma^{\rm FIX-C}$.

The dark energy parameter constraints with prior knowledge of effective concentrations is shown in Figure 11. As before, LSST is the most sensitive to concentration variations and can reap significant benefit from priors on the $c(m,z)$ relation. In the LSST case, prior constraints on the concentration relation at redshift $z = 0$ have little effect if they are greater than the $\sim 30\%$ level. This is sensible because LSST itself would constrain concentrations in the relevant mass range at this level in the absence of prior knowledge. Naturally, prior constraints on $c(m,z)$ that are better than $\sim 30\%$ lead to rapid decreases in parameter uncertainties with decreasing $\delta_{\rm c}$ in each case.

The behavior of parameter constraints as a function of prior reflects the details of each of the experiments. An experiment with enormous sky coverage, such as LSST, can establish the amplitude of large-scale density fluctuations and the cosmic distance scale with low-multipole information and information from the high-redshift tomographic bins rather effectively, so that such an experiment can take advantage of decreases in $\delta_{\rm c}$ even with no prior on β. This statement is less true for SNAP and DES because these experiments have a relatively shorter lever arm in multipoles over which to derive constraints. SNAP is limited by its comparably small sky coverage and DES by its comparable shallowness. As the prior constraints on β improve, both DES and SNAP become increasingly capable of exploiting prior knowledge of the amplitude of the $c(m,z)$ relation as can be seen for $\delta_{\rm c} \lesssim 0.25$ in the two rightmost columns of Fig. 11. In the case of LSST, the figure of merit increases with

decreasing δ_c less rapidly than one might suppose based solely on the marginalized uncertainties in w_0 and w_a because in this case the correlation between parameters varies strongly with δ_c.

In summary, the dark energy constraints from an experiment such as LSST can benefit greatly from prior knowledge of the effective concentrations of halos that are better than $\sim 25\%$, while constraining the redshift evolution parameter β, of concentrations to better than $\sim 30\%$ leads to a rapid decrease in constraints in the absence of prior knowledge of the amplitude of the $c(m,z)$ relation. For DES and SNAP, it is necessary to constrain the redshift evolution of $c(m,z)$ before either of these experiments can exploit prior knowledge of the amplitude of the $c(m,z)$ relation effectively. In the cases we study, this requires prior knowledge of the β parameter to better than $\sim 20\%$. Knowing the amplitude of the concentration relation would reduce parameter degradation to less than $\sim 20\%$ in the case of LSST, while knowing both the amplitude and the redshift parameter β to less than $\sim 20\%$ would reduce parameter degradation to less than $\sim 10\%$ for all experiments.

IV. SUMMARY AND DISCUSSION

We have studied the ability of forthcoming weak lensing surveys to constrain both dark energy properties and the concentrations of dark matter halos simultaneously. The primary motivations for this work are recent studies demonstrating that baryonic physics, neglected in prior forecasting of weak lensing constraints on dark energy properties, have a considerable influence on predictions for convergence power spectra [27, 28]. Moreover, the large enhancements in convergence spectra predicted by these hydrodynamic simulations arose primarily from modifications in the internal structures of halos [28]. Clearly, gravitational lensing is sensitive to all matter so here, as in the rest of the paper, we refer to halo concentrations, but by this we mean the effective concentrations of composite systems comprised of dark matter and baryons in radial range $0.04 \lesssim r/R_{200\mathrm{m}} \lesssim 1$. We have shown that neglecting these baryonic effects can lead to large biases in inferred dark energy parameters unless information from multipoles greater than a few hundred is disregarded (see Fig. 3). On the other hand, weak lensing surveys have the ability to self calibrate for the effects baryons as an alternative to eliminating small-scale information.

We modeled the unknown relationship between effective concentration and halo mass in two different ways. In the more restrictive set of models, we considered concentration as a power-law function of halo mass. As we have demonstrated, convergence spectra are most sensitive to halo concentrations in a relatively narrow range of halo masses near a few $\times 10^{14}\ h^{-1}\mathrm{M}_\odot$, so this class of models may not be overly restrictive. Nevertheless, in currently-favored cosmological models, the mass-to-light ratios of halo systems must be a non-monotonic function of halo mass, so it is desirable to study relations with more freedom. Along these lines, we studied binned relationships between concentration and halo mass specified by average concentration values at a fixed number of halo masses, evenly spaced in the logarithm of the halo mass between $11 \leq \log(M/\ h^{-1}\mathrm{M}_\odot) \leq 16$. In these models, we used spline interpolation to obtain halo concentrations between the values of halo mass at which the concentrations were specified. Throughout this paper, we have presented results for a concentration-mass relationship specified at five bins in this mass interval, but have verified that our results are relatively insensitive to the number of bins up to about twelve bins. Coupled with our prejudice that these effective concentrations will likely be very smooth functions of halo mass, this class of model is likely to have sufficient flexibility to produce the types of mass-concentration relations that are realized in nature. In both cases, we allowed for a redshift dependence to the modification in the halo mass-concentration relation by taking $c(m,z) = c(m,z=0)/(1+z)^\beta$.

Our study implies that self-calibration is a quite promising alternative to simply eliminating multipoles beyond which significant parameter biases may be likely. Comparing constraints obtained by removing multipoles beyond a few hundred with constraints that include all multipoles up to $\ell = 3000$ and assume perfect knowledge of halo concentrations, the degradation in parameter uncertainties is a factor of $\sim 1.5 - 3$. The details of the degradation depend upon the parameter of interest, the experiment, and the fiducial cosmological model. As it is the most sensitive of the forthcoming instruments on large scales, the requirements for LSST to be unbiased are the most restrictive and indicate that multipoles beyond ~ 300 should not be considered in parameter extraction. The corresponding degradation in parameter constraints for LSST is a factor of ~ 3 for all parameters. On the contrary, our study suggests that self calibration is a more fruitful alternative. Even in our most permissive concentration models, dark energy parameter constraints from this self-calibration exercise are never degraded by more than 36% and more restrictive models (if they can be justified) do significantly better. In particular, if the concentration-mass relation can be constrained to better than 20% at a specific redshift, the constraints derived from an LSST-like experiment will be degraded by only $\sim 20\%$. If, in addition, the power-law index describing the redshift evolution of effective halo concentrations is also known to within 20%, then dark energy parameter constraints will be degraded by no more than $\sim 10\%$ for any of LSST, DES, or SNAP individually.

Self calibration as an alternative to removing the information contained in high-ℓ multipoles has another advantage; it provides direct constraints on halo concentrations that may complement, if not be competitive with, other methods. In the case of the power-law class of models for effective halo concentrations as a function of mass and redshift, LSST alone can constrain halo con-

centrations near the pivot mass, $m_{\rm piv} \sim 10^{14}\ h^{-1}{\rm M}_\odot$, and redshift, $z_{\rm piv} \sim 0.2$, at the $\sim 5\%$ level with only modest prior constraints on cosmology that are typical of our contemporary knowledge of cosmological parameters. Both DES and SNAP constrain halo concentrations at the pivot mass and redshift to about $\sim 10\%$. Generalizing to the case of the arbitrary, binned relation for halo concentrations, LSST alone constrains halo concentrations near $m \sim 3 \times 10^{14}\ h^{-1}{\rm M}_\odot$ to within 48%. Adding prior constraints on cosmological parameters from the Planck cosmic microwave background satellite and supernova luminosity distances as measured from SNAP reduce this to a 30% constraint. Though modest, this constraint would not be subject to the same systematics and selection issues as other techniques.

Our work has several shortcomings. Of course, our framework for all of these calculations has been the halo model, and this phenomenological model has known inadequacies. More importantly, we have modeled the effect of baryons as entirely restricted to the internal structures of halos. Though this is a good approximation in current simulations [28], it is unreasonable to expect that this is strictly true and no study has yet addressed potentially-important, though sub-dominant, additional modification to matter power spectra. Changes to the detailed profile shapes, and the mass function of halos (already measured in Ref. [28]), the clustering of halos are all likely to be important at some level. To address this issue is an ambitious goal which lies well beyond the scope of our study, yet it is a goal that must be achieved in order to take full advantage of these forthcoming experiments. The degree to which baryons will modify the matter power spectra will likely remain uncertain for some time, yet we must at least enumerate the different ways in which the power spectra are modified. As an example, the study of Ref. [28] does show percent-level residuals between their simulation results and the results of a model based entirely on modified halo concentrations. Although the results of Ref. [28] are noisy due to their small simulation volume, we can use their data to obtain a first guess at the residual bias that may remain after allowing for variation in halo concentration parameters. Our estimates suggest that in the case of LSST the bias is a few percent of the 1σ parameter uncertainty at $\ell_{\rm max} = 10^3$ and is of order $|\delta|/\sigma \simeq 0.1$ at $\ell_{\rm max} = 3000$ for both w_0 and $w_{\rm a}$. The residual biases in the case of DES and SNAP are smaller yet. Furthermore, we have described forthcoming experiments in a simple manner and so detailed comparisons between the projected performances of instruments based on this study should not be regarded as definitive. Certainly, systematic issues regarding shape measurements will be better controlled in space-borne instruments like SNAP than from the ground. Moreover, SNAP with potentially much greater depth than either DES or LSST will be sensitive to relatively higher-redshift, larger-scale fluctuations at a fixed angular scale. On such scales, the fluctuation spectrum will be less subject to nonlinear effects. Lastly, we have ignored all additional systematics whether theoretical or observational. We anticipate that in the years leading up to the surveys we have studied, a considerable amount of effort will be put into making theoretical predictions more accurate. We expect — or at least hope — that more sophisticated methods for predicting matter power spectra will supplant current techniques and find it most likely that the parameterizations we adopted will not be those that are implemented in the actual data analyses. Nevertheless, our study gives a preliminary indication that calibration of uncertain baryonic effects will be possible at minimal cost and that this calibration may provide interesting information about halo structure that may be used to diagnose models of the evolution of the baryons themselves.

In the context of our models, calibrating effective halo concentrations in parallel with deriving constraints on dark energy parameters is extremely successful and the preceding paragraph is not intended to undercut our primary results and conclusions. We are optimistic that this success will carry over to more complex models that may include systematics and additional modifications to power spectra due to baryonic processes. Part of our optimism stems directly from the success with which halo structure can be calibrated, as we have demonstrated here. In addition, we are optimistic because we have used only a fraction of the information contained within these surveys. In particular, we restricted our analysis to multipoles $\ell < 3000$ in order to remain in the regime where Gaussian statistics and other weak lensing approximations are valid. Accounting for non-Gaussianity and dropping additional assumptions, such as the Born approximation and the use of reduced shear [66], would allow higher multipoles to be included in the analysis. This would greatly increase the constraining power of these week lensing surveys. More specifically, SNAP is the deepest survey we have considered by a large margin. As such, SNAP suffers the most from setting $\ell_{\rm max} = 3000$ and going beyond this limit would enable SNAP to outperform the projections we present here (while systematics will also be better controlled from space). An important implication of this is that upon extending the analysis to small scales, SNAP would provide the best determination of baryonic effects, eliminating degeneracies that may limit dark energy constraints. Of course, gains from small-scale observations would also come with the challenge of predicting power spectra out to higher multipoles. Furthermore, we have used only weak lensing shear information and have not utilized the galaxy power spectra and galaxy-shear cross spectra that would also be contained within these surveys and would make these constraints more robust [69, 84]. Our study shows the great promise of future surveys to constrain dark energy along with numerous other phenomena, but is is only the tip of the iceberg and we must meet several theoretical challenges in order to exploit the enormous amount of information that will be available in forthcoming photometric surveys.

Acknowledgments

We are grateful to Gary Bernstein, Dragan Huterer, Andrey Kravtsov, Zhaoming Ma, Brant Robertson, Chaz Shapiro, Louie Strigari, Jeremy Tinker, Sheng Wang, Martin White, and Hu Zhan for many useful discussions. This work was supported by the Kavli Institute for Cosmological Physics at The University of Chicago under the NSF Physics Frontier Grant NSF PHY 0114422. ARZ has been additionally funded by the University of Pittsburgh and the National Science Foundation (NSF) Astronomy and Astrophysics Postdoctoral Fellowship program through grant AST 0602122. WH was additionally supported by the U.S. Dept. of Energy contract DE-FG02-90ER-40560 and the David and Lucile Packard Foundation. This work made use of the National Aeronautics and Space Administration Astrophysics Data System.

[1] A. G. Riess, A. V. Filippenko, P. Challis, and et al., Astron. J. **116**, 1009 (1998), astro-ph/9805201.
[2] S. Perlmutter, G. Aldering, G. Goldhaber, and et al., Astrophys. J. **517**, 565 (1999), astro-ph/9812133.
[3] M. Tegmark, M. A. Strauss, M. R. Blanton, and et al., Phys. Rev. D **69**, 103501 (2004), astro-ph/0310723.
[4] A. G. Riess, L.-G. Strolger, J. Tonry, S. Casertano, H. C. Ferguson, B. Mobasher, P. Challis, A. V. Filippenko, S. Jha, W. Li, et al., Astrophys. J. **607**, 665 (2004), astro-ph/0402512.
[5] D. J. Eisenstein, I. Zehavi, D. W. Hogg, and et al., Astrophys. J. **633**, 560 (2005), astro-ph/0501171.
[6] D. N. Spergel, R. Bean, O. Doré, M. R. Nolta, C. L. Bennett, J. Dunkley, G. Hinshaw, N. Jarosik, E. Komatsu, L. Page, et al., Astrophys. J. Suppl. Ser. **170**, 377 (2007), arXiv:astro-ph/0603449.
[7] M. Tegmark, D. J. Eisenstein, M. A. Strauss, and et al., Phys. Rev. D **74**, 123507 (2006), astro-ph/0608632.
[8] P. Astier, J. Guy, N. Regnault, and et al., Astron. Astrophys. **447**, 31 (2006), astro-ph/0510447.
[9] W. M. Wood-Vasey, G. Miknaitis, C. W. Stubbs, and et al., Astrophys. J. submitted (astro-ph/0701041) (2007), astro-ph/0701041.
[10] W. Hu and M. Tegmark, Astrophys. J. Lett. **514**, L65 (1999), astro-ph/9811168.
[11] W. Hu, Astrophys. J. Lett. **522**, L21 (1999), astro-ph/9904153.
[12] D. Huterer, Phys. Rev. D **65**, 063001 (2002), astro-ph/0106399.
[13] A. Heavens, Mon. Not. R. Astron. Soc. **343**, 1327 (2003), astro-ph/0304151.
[14] A. Refregier, Ann. Rev. Astron. Astroph. **41**, 645 (2003), astro-ph/0307212.
[15] A. Refregier, R. Massey, J. Rhodes, R. Ellis, J. Albert, D. Bacon, G. Bernstein, T. McKay, and S. Perlmutter, Astron. J. **127**, 3102 (2004), astro-ph/0304419.
[16] Y.-S. Song and L. Knox, Phys. Rev. D **70**, 063510 (2004), astro-ph/0312175.
[17] M. Takada and B. Jain, Mon. Not. R. Astron. Soc. **348**, 897 (2004), astro-ph/0310125.
[18] M. Takada and M. White, Astrophys. J. Lett. **601**, L1 (2004), astro-ph/0311104.
[19] S. Dodelson and P. Zhang, Phys. Rev. D **72**, 083001 (2005), astro-ph/0501063.
[20] A. Albrecht, G. Bernstein, R. Cahn, W. L. Freedman, J. Hewitt, W. Hu, J. Huth, M. Kamionkowski, E. W. Kolb, L. Knox, et al., (astro-ph/0609591) (2006), astro-ph/0609591.
[21] H. Zhan, Journal of Cosmology and Astro-Particle Physics **8**, 8 (2006), astro-ph/0605696.
[22] D. Huterer and M. Takada, Astroparticle Physics **23**, 369 (2005), astro-ph/0412142.
[23] D. Huterer, M. Takada, G. Bernstein, and B. Jain, Mon. Not. R. Astron. Soc. **366**, 101 (2006), astro-ph/0506030.
[24] K. Heitmann, P. M. Ricker, M. S. Warren, and S. Habib, Astrophys. J. Suppl. Ser. **160**, 28 (2005), astro-ph/0411795.
[25] M. White, Astroparticle Physics **22**, 211 (2004), astro-ph/0405593.
[26] H. Zhan and L. Knox, Astrophys. J. Lett. **616**, L75 (2004), astro-ph/0409198.
[27] Y. P. Jing, P. Zhang, W. P. Lin, L. Gao, and V. Springel, Astrophys. J. Lett. **640**, L119 (2006), astro-ph/0512426.
[28] D. H. Rudd, A. R. Zentner, and A. V. Kravtsov, Astrophys. J. Submitted (2007), astro-ph/0703741.
[29] E. S. Sheldon, D. E. Johnston, J. A. Frieman, R. Scranton, T. A. McKay, A. J. Connolly, T. Budavári, I. Zehavi, N. A. Bahcall, J. Brinkmann, et al., Astron. J. **127**, 2544 (2004), arXiv:astro-ph/0312036.
[30] E. L. Łokas, R. Wojtak, S. Gottlöber, G. A. Mamon, and F. Prada, Mon. Not. R. Astron. Soc. **367**, 1463 (2006), arXiv:astro-ph/0511723.
[31] R. Mandelbaum, U. Seljak, R. J. Cool, M. Blanton, C. M. Hirata, and J. Brinkmann, Mon. Not. R. Astron. Soc. **372**, 758 (2006), arXiv:astro-ph/0605476.
[32] D. A. Buote, F. Gastaldello, P. J. Humphrey, L. Zappacosta, J. S. Bullock, F. Brighenti, and W. G. Mathews, (astro-ph/0610135) (2006), astro-ph/0610135.
[33] A. S. Bolton, S. Burles, L. V. E. Koopmans, T. Treu, and L. A. Moustakas, Astrophys. J. **638**, 703 (2006), arXiv:astro-ph/0511453.
[34] D. E. Johnston, E. S. Sheldon, A. Tasitsiomi, J. A. Frieman, R. H. Wechsler, and T. A. McKay, Astrophys. J. **656**, 27 (2007), arXiv:astro-ph/0507467.
[35] R. Gavazzi, T. Treu, J. D. Rhodes, L. V. E. Koopmans, A. S. Bolton, S. Burles, R. Massey, and L. A. Moustakas, (astro-ph/0701589) (2007), astro-ph/0701589.
[36] J. M. Comerford and P. Natarajan, (astro-ph/0703126) (2007), astro-ph/0703126.
[37] C. M. Hirata and U. Seljak, Phys. Rev. D **70**, 063526 (2004), arXiv:astro-ph/0406275.
[38] C. Heymans, M. Brown, A. Heavens, K. Meisenheimer, A. Taylor, and C. Wolf, Mon. Not. R. Astron. Soc. **347**, 895 (2004), arXiv:astro-ph/0310174.
[39] R. Mandelbaum, C. M. Hirata, M. Ishak, U. Seljak, and J. Brinkmann, Mon. Not. R. Astron. Soc. **367**, 611 (2006), arXiv:astro-ph/0509026.
[40] S. Bridle and L. King, ArXiv e-prints **705** (2007),

0705.0166.
[41] A. Albrecht, G. Bernstein, R. Cahn, W. L. Freedman, J. Hewitt, W. Hu, J. Huth, M. Kamionkowski, E. W. Kolb, L. Knox, et al., ArXiv Astrophysics e-prints (2006), astro-ph/0609591.
[42] Z. Ma, W. Hu, and D. Huterer, Astrophys. J. **636**, 21 (2006), astro-ph/0506614.
[43] J. A. Peacock and S. J. Dodds, Mon. Not. R. Astron. Soc. **280**, L19 (1996), arXiv:astro-ph/9603031.
[44] R. E. Smith, J. A. Peacock, A. Jenkins, S. D. M. White, C. S. Frenk, F. R. Pearce, P. A. Thomas, G. Efstathiou, and H. M. P. Couchman, Mon. Not. R. Astron. Soc. **341**, 1311 (2003), astro-ph/0207664.
[45] R. J. Scherrer and E. Bertschinger, Astrophys. J. **381**, 349 (1991).
[46] C.-P. Ma and J. N. Fry, Astrophys. J. **543**, 503 (2000), astro-ph/0003343.
[47] U. Seljak, Mon. Not. R. Astron. Soc. **318**, 203 (2000).
[48] R. Scoccimarro, R. K. Sheth, L. Hui, and B. Jain, Astrophys. J. **546**, 20 (2001).
[49] R. K. Sheth, H. J. Mo, and G. Tormen, Mon. Not. R. Astron. Soc. **323**, 1 (2001), astro-ph/9907024.
[50] A. Cooray and R. Sheth, Phys. Rep. **372**, 1 (2002).
[51] D. J. Eisenstein and W. Hu, Astrophys. J. **511**, 5 (1999), astro-ph/9710252.
[52] W. Hu, Phys. Rev. D **66**, 083515 (2002), arXiv:astro-ph/0208093.
[53] J. L. Tinker, D. H. Weinberg, and M. S. Warren, Astrophys. J. **647**, 737 (2006), astro-ph/0603146.
[54] J. F. Navarro, C. S. Frenk, and S. D. M. White, Astrophys. J. **490**, 493 (1997), astro-ph/9611107.
[55] J. S. Bullock, T. S. Kolatt, Y. Sigad, R. S. Somerville, A. V. Kravtsov, A. A. Klypin, J. R. Primack, and A. Dekel, Mon. Not. R. Astron. Soc. **321**, 559 (2001), astro-ph/9908159.
[56] K. Dolag, M. Bartelmann, F. Perrotta, C. Baccigalupi, L. Moscardini, M. Meneghetti, and G. Tormen, Astron. Astrophys. **416**, 853 (2004).
[57] A. V. Macciò, A. A. Dutton, F. C. van den Bosch, B. Moore, D. Potter, and J. Stadel, Mon. Not. R. Astron. Soc. **378**, 55 (2007), arXiv:astro-ph/0608157.
[58] R. H. Wechsler, A. R. Zentner, J. S. Bullock, A. V. Kravtsov, and B. Allgood, Astrophys. J. **652**, 71 (2006), astro-ph/0512416.
[59] A. F. Neto, L. Gao, P. Bett, S. Cole, J. F. Navarro, C. S. Frenk, S. D. M. White, V. Springel, and A. Jenkins, ArXiv e-prints **706** (2007), 0706.2919.
[60] W. Hu and A. V. Kravtsov, Astrophys. J. **584**, 702 (2003), arXiv:astro-ph/0203169.
[61] A. Cooray and W. Hu, Astrophys. J. **554**, 56 (2001), astro-ph/0012087.
[62] D. Dolney, B. Jain, and M. Takada, Mon. Not. R. Astron. Soc. **352**, 1019 (2004), arXiv:astro-ph/0401089.
[63] R. K. Sheth and G. Tormen, Mon. Not. R. Astron. Soc. **308**, 119 (1999), astro-ph/9901122.
[64] M. White and W. Hu, Astrophys. J. **537**, 1 (2000).
[65] C. Vale and M. White, Apj **592**, 699 (2003).
[66] S. Dodelson, C. Shapiro, and M. White, Phys. Rev. D **73**, 023009 (2006), arXiv:astro-ph/0508296.
[67] E. Semboloni, L. van Waerbeke, C. Heymans, T. Hamana, S. Colombi, M. White, and Y. Mellier, Mon. Not. R. Astron. Soc. **375**, L6 (2007), arXiv:astro-ph/0606648.
[68] D. Huterer and M. S. Turner, Phys. Rev. D **64**, 123527 (2001), arXiv:astro-ph/0012510.
[69] W. Hu and B. Jain, Phys. Rev. D **70**, 043009 (2004), arXiv:astro-ph/0312395.
[70] N. Katz and S. D. M. White, Astrophys. J. **412**, 455 (1993).
[71] G. F. Lewis, A. Babul, N. Katz, T. Quinn, L. Hernquist, and D. H. Weinberg, Astrophys. J. **536**, 623 (2000), astro-ph/9907097.
[72] F. R. Pearce, P. A. Thomas, H. M. P. Couchman, and A. C. Edge, Mon. Not. R. Astron. Soc. **317**, 1029 (2000), astro-ph/9908062.
[73] R. Davé, R. Cen, J. P. Ostriker, G. L. Bryan, L. Hernquist, N. Katz, D. H. Weinberg, M. L. Norman, and B. O'Shea, Astrophys. J. **552**, 473 (2001), astro-ph/0007217.
[74] M. L. Balogh, F. R. Pearce, R. G. Bower, and S. T. Kay, Mon. Not. R. Astron. Soc. **326**, 1228 (2001), astro-ph/0104041.
[75] S. Borgani, F. Governato, J. Wadsley, N. Menci, P. Tozzi, T. Quinn, J. Stadel, and G. Lake, Mon. Not. R. Astron. Soc. **336**, 409 (2002), astro-ph/0205471.
[76] T. Suginohara and J. P. Ostriker, Astrophys. J. **507**, 16 (1998), astro-ph/9803318.
[77] A. Cooray, W. Hu, and J. Miralda-Escude, Astrophys. J. **535**, L9 (2000), astro-ph/0003205.
[78] N. A. Bahcall, R. Cen, R. Davé, J. P. Ostriker, and Q. Yu, Astrophys. J. **541**, 1 (2000), arXiv:astro-ph/0002310.
[79] J. L. Tinker, D. H. Weinberg, Z. Zheng, and I. Zehavi, Astrophys. J. **631**, 41 (2005), astro-ph/0411777.
[80] F. C. van den Bosch, X. Yang, H. J. Mo, S. M. Weinmann, A. V. Macciò, S. More, M. Cacciato, R. Skibba, and X. Kang, Mon. Not. R. Astron. Soc. **376**, 841 (2007), arXiv:astro-ph/0610686.
[81] D. N. Spergel, L. Verde, H. V. Peiris, E. Komatsu, M. R. Nolta, C. L. Bennett, M. Halpern, G. Hinshaw, N. Jarosik, A. Kogut, et al., Astrophys. J. Suppl. Ser. **148**, 175 (2003), arXiv:astro-ph/0302209.
[82] D. Huterer and M. White, Phys. Rev. D **72**, 043002 (2005), arXiv:astro-ph/0501451.
[83] W. Hu, D. Huterer, and K. M. Smith, Astrophys. J. Lett. **650**, L13 (2006), arXiv:astro-ph/0607316.
[84] G. M. Bernstein and B. Jain, Astrophys. J. **600**, 17 (2004), astro-ph/0309332.
[85] URL http://www.mpa-garching.mpg.de/galform/virgo/millennium/
[86] URL http://www.darkenergysurvey.org
[87] URL http://snap.lbl.gov
[88] URL http://www.lsst.org
[89] The difference in numerical factors reported here reflects the difference between the halo definition used in Ref. [28] and the one we use in this study. We have converted between the two definitions as described in Ref. [60].